The Dawn of Chemistry

Daniele Galli, Francesco Palla
INAF-Osservatorio Astrofisico di Arcetri
Largo E. Fermi 5, 50125 Firenze, Italy

email: galli,palla@arcetri.astro.it

To appear in Annual Reviews of Astronomy and Astrophysics Volume 51

Key Words Early Universe, Primordial Chemistry, Atomic and Molecular Processes, Population III stars, Cosmology

Abstract
Within the precise cosmological framework provided by the Λ-Cold Dark Matter model and standard Big Bang nucleosynthesis, the chemical evolution of the pregalactic gas can now be followed with accuracy limited only by the uncertainties on the reaction rates. Starting during the recombination era, the formation of the first molecules and molecular ions containing hydrogen, deuterium, helium, and lithium was severely hindered by the low density of the expanding universe, the intensity of the cosmic radiation field, and the absence of solid catalyzers. Molecular hydrogen and deuterated hydrogen, the most abundant species formed in the gas phase prior to structure formation, played a fundamental role in the cooling of the gas clouds that gave birth to the first stellar generation, contributing to determine the scale of fragmentation. Primordial molecules also interacted with the photons of the cosmic background via resonant scattering, absorption and emission. In this review we examine the current status of the chemistry of the early universe and discuss the most relevant reactions for which uncertainties still exist from theory or laboratory experiments. The prospects for detecting spectral distortions or spatial anisotropies due to the first atoms and molecules are also addressed.

CONTENTS

1 PRESENT CONTEXT AND MOTIVATIONS

We live in a chemically and dynamically evolving universe. The interplay between these two domains has shaped the universe in the way we observe it now. Dynamics, driven by visible and invisible forces, has governed the transformation of minute density perturbations into structures of varying degree of complexity (from galaxies to individual stars within them). Chemistry has been instrumental for modifying a very simple mixture of nuclei and electrons into complex molecules and solid particles, the essential ingredients for cooling and fragmentation of the interstellar gas. This review is an account of the portion of the chemical evolution that spanned a small fraction of the universe's lifetime, between the recombination era at redshift $z \approx 1000$ when it was only 380,000 years old and the transitional phase of cosmic re-ionization at redshifts $z \approx 15$–6. This epoch is commonly called the "dark ages" since it preceded – or, more precisely, included the beginning of – the formation of the first structures, which were either individual stars (or groups of stars) of the Population III, or an entire generation of stars within pre-galactic gas clouds. The radiation of these stellar objects lit up the sky and contributed significantly to the re-ionization of the intergalactic gas, a process that was basically completed by a redshift of $z \approx 6$ at an age of ~ 800 million years.

The first synthesis of the elements, mainly nucleons, occurred in a very short time interval approximately three minutes after the initial expansion of the universe, but it took about four hundred thousand years before conditions were suitable for matter and radiation to decouple, with the former recombining into neutral atoms. However, recombination lagged behind expansion and at a redshift of $z \approx 800$ a minute fraction of electrons and protons froze out at a level of one part in $\sim 10^4$. The rapidly varying level of ionization, along with the ever decreasing energy of the photons of the cosmic microwave background (CMB) radiation, effectively promoted the formation of the first molecular species, ions and neutrals, that survived the processes of photoionization/photodissociation and dissociative recombination. This was, in fact, the "dawn of chemistry".

Since Big Bang nucleosynthesis produced hydrogen and helium (along with their isotopes), with trace abundances of Li Be B and no solid particles, chemical reactions in the low density medium of the expanding universe only occurred in

the gas phase. Therefore, the first molecules and molecular ions were quite simple and limited to few dominant species, such as H_2, HD, HeH^+, and LiH (Lepp & Shull 1984). The search for these species prior to structure formation, either directly in the pregalactic medium or through their effects on the spectrum of the CMB has proved as yet unsuccessful in spite of several efforts (de Bernardis et al. 1993; Persson et al. 2010). Owing to its potential role in primordial chemistry and in the cooling of the gas, LiH has also been searched for towards high redshift QSOs. Recent observations by Friedel, Kemball & Fields (2011) with the CARMA array of the $J = 0 - 1$ transition of ^{7}LiH and ^{6}LiH have resulted in a 3σ-level detection of ^{7}LiH only in the source B0218+357 ($z_{\rm abs} = 0.685$), confirming an earlier claim by Combes & Wiklind (1998). Similarly, a tentative detection of the $J = 1 - 0$ rotational line of HeH^+ has been made towards one of the highest redshift quasars at $z = 6.4$ where other molecular lines had been previously detected (Zinchenko, Dubrovich & Henkel 2011).

Another obstacle in probing the physical conditions of the gas during the dark ages is that measurements towards high redshift galaxies and the diffuse gas have largely failed to identify clouds of primordial composition. On the contrary, there appears to be a systematic contamination by heavy elements at levels of $Z \approx 10^{-3}$ of the solar abundance (e.g., Wolfe, Gawiser & Prochaska 2005) which appears to extend up to $z \sim 5$ and which implies enrichment from the ejecta of earlier generations of stars (Rafelsky et al. 2012). However, recent studies have identified gas clouds without any trace of heavy elements or with metallicities consistent with enrichment by primordial stars (Fumagalli, O'Meara & Prochaska 2011; Cooke, Pettini & Steidel 2011). Interestingly, the pristine clouds LLS1134a and LLS0956B with $Z < 10^{-4}\ Z_\odot$ at $z \approx 3$ identified by Fumagalli, O'Meara & Prochaska (2011) are located in regions of density significantly higher than the background, but unpolluted by heavy elements, indicating that mixing of the metals in the intergalactic medium is both inhomogeneous and inefficient.

Finally, although a genuine zero-metal star has so far escaped detection, the search for such objects proceeds unabated due to the unique information that they carry about the earliest phases of galactic formation and evolution (e.g., Yong et al. 2012). The most exciting discovery of the last few years is the low-mass star of the galactic halo SDSS J102915+172927 with a metallicity 4.5×10^{-5} times that of the Sun and without enrichment of C, N, O (Caffau et al. 2011,2012). Although a number of stars of extremely low metallicity had been previously detected, they all showed significant overabundance of the heavy elements, a signature of pollution by a previous generation of massive stars (Frebel et al. 2008; Christlieb et al. 2002; Norris et al. 2007). From the analysis of their sample, Caffau et al. (2011) conclude that SDSS J102915 is not an isolated object and that a significant number of similar, or of even lower metallicity, low-mass stars will be discovered in the near future. These findings will definitely clarify the issue on the existence of a transition in the mass scale of the stars formed in the primordial universe. While a transition from massive to low-mass fragments based on the cooling properties of atomic lines of OI, CII, SiII and FeII and on the existence of a critical value of the C/H and O/H abundance has been suggested for some time (Bromm & Loeb 2003, Frebel, Johnson & Bromm 2007), the discovery of SDSS J102915 with metal abundance below the critical value appears to favor the view of a transition based on the cooling properties of dust formed in the ejecta of core-collapse SNe of the first generation (e.g., Schneider et al. 2012; Klessen, Glover & Clark 2012).

The exciting developments in the search for primordial molecules, clouds and stars outlined above make a review of the critical chemical processes that took place in the post-recombination universe timely. Until recently, large uncertainties existed not only on the rates of some key chemical reactions, but also (and, to some extent, more significantly) on the cosmological model and its fundamental parameters, and on the yields from Big Bang nucleosynthesis (BBN). The advent of precision cosmology and a concordance model, along with significant improvements in standard BBN calculations offer accurate initial and boundary conditions for the study of the chemistry of the primordial gas, so that much of the remaining uncertainty resides in the poor knowledge of some basic reactions. Therefore, a coherent picture of the chemistry of the main constituents (hydrogen, deuterium, helium, and lithium) can be provided and, hopefully, tested.

In this review, we will cover the post-recombination epoch in the unperturbed universe prior to the development of the first structures, whether individual stars or galaxies. Once these objects form, feedback effects and chemical enrichment become extremely important and need to be taken into account for a consistent treatment of the interstellar/intergalactic medium. Thus, the chemistry will be very different from that described here and an appropriate discussion would require a dedicated review. Similarly, the problem of the fragmentation and collapse of primordial clouds and the characteristic properties of the first stars will only be addressed in the light of the chemical properties of the gas. This field of research has made considerable progress in recent years thanks to the development of highly sophisticated numerical simulations and excellent summaries can be found in the literature (e.g., Bromm et al. 2009; Bromm & Yoshida 2011; Loeb 2010; Umemura & Omukai 2013).

The organization of this review is as follows: we sketch in Section 2 the early motivations to study the formation of molecular hydrogen and other molecules in the cosmological context. A good recipe for the chemical evolution of the primordial gas requires the specification of the main ingredients (a cosmological model, the abundance of the light elements from nucleosynthesis, the ionization history through recombination) and this will be provided in Section 3. Section 4 will present the results of the calculations of the predicted abundances of the main molecules and molecular ions, along with a discussion of the most critical reaction rates. The effects of chemistry on the cooling of the primordial gas will be highlighted in Section 5. Once formed, molecules as well as atoms can interact with the CMB and possibly leave some imprints both as spectral distortions and spatial anisotropies and Section 6 will address this important aspect. Finally, a summary of the major issues (Section 7) and some future perspectives (Section 8) on both theoretical and observational studies of primordial chemistry will close the review.

2 EARLY DEVELOPMENTS

The investigation of the role of molecular hydrogen as an important coolant for the formation of the first structures in the early universe began in the late 1960s. Saslaw & Zipoy (1967) were the first to point out the important role of H_2 molecules for the thermal and dynamical evolution of pre-galactic gas clouds in the post-recombination era. Unlike previous attempts that had ignored the possible presence of H_2 molecules due to the lack of dust grains and the slow rate

of radiative association and three body reactions, Saslaw & Zipoy considered the possibility of radiative association and charge transfer reactions such as[1]

$$\mathrm{H} + \mathrm{H}^+ \rightarrow \mathrm{H}_2^+ + h\nu \tag{1}$$

and

$$\mathrm{H}_2^+ + \mathrm{H} \rightarrow \mathrm{H}_2 + \mathrm{H}^+. \tag{2}$$

The rate constant for reaction (1) was taken from a calculation by Bates (1951), while the cross section for reaction (2) was estimated to have a relatively high value of $\sim 10^{-15}$ cm^2, typical of charge exchange reactions above threshold. Thus, an H_2^+ ion can be converted to H_2 as soon as it is formed and the H_2^+ concentration remains very low. In addition, owing to the low electron abundance, dissociative recombination of H_2^+ turned out to be negligible compared with reaction (2) and H_2 molecules could then be formed at a significant rate. Using the radiative cooling function calculated by Takayanagi & Nishimura (1960), Saslaw & Zipoy (1967) showed that, under reasonable assumptions for the initial conditions of the collapsing clouds, their evolution would depart from pure adiabatic collapse at densities above $\sim 10^4$ cm^{-3} due to enhanced H_2 formation and cooling. Cloud contraction could then proceed at high densities before the onset of optical depth effects and H_2 collisional dissociation, thus allowing the formation of stars of unspecified characteristics. Saslaw & Zipoy suggested that the resulting object might resemble a globular cluster.

Peebles & Dicke (1968) also considered the origin of globular clusters prior to the formation of galaxies. They noticed the correspondence between the characteristic mass and size of the first generation of bound systems, given by the Jeans mass and length ($\sim 10^5\ M_\odot$ and ~ 5 pc, respectively), and that of globular clusters. However, Peebles & Dicke relied on another channel for efficient H_2 formation and cooling provided by the presence of negative hydrogen ions. They referred to McDowell (1961) who calculated the H_2 abundance in the interstellar medium, following an earlier private communication by Dalgarno (1958)[2]. In this scheme, H_2 formation proceeds through the reactions

$$\mathrm{H} + e \rightarrow \mathrm{H}^- + h\nu \tag{3}$$

and

$$\mathrm{H}^- + \mathrm{H} \rightarrow \mathrm{H}_2 + e. \tag{4}$$

The rate coefficient for (3) was calculated from the cross section given by Chandrasekhar (1958), while that for reaction (4) was based on laboratory measurements by Schmeltekopf, Fehsenfeld & Ferguson (1967). Once again, since the rate for (4) is much more rapid than for (3), the formation of a negative hydrogen is promptly followed by the conversion to a hydrogen molecule. In addition, this route is faster than that through H_2^+ formation (by a factor of $\sim$100 at 1000 K),

[1]They acknowledge P. Solomon, private communication

[2]Pagel (1959) was the first to point out the H^- channel for H_2 formation in the solar photosphere, acknowledging A. Dalgarno for the suggestion. Later, McDowell (1961) calculated the H_2 fractional abundance in HI regions, quoting Pagel's calculation for the Sun and Dalgarno's estimate for the rate coefficient. Interestingly, McDowell mentions the fact that McCrea (1960) had pointed out that "consideration of the problem of star formation in HI regions strongly suggests that the hydrogen is present in molecular form". McDowell did not consider 3-body reactions because of the low densities, while McCrea & McNally (1960) suggested that the mechanism for H_2 formation could be that of surface reactions on dust grains.

so that the latter was neglected in the calculations. The efficient formation of H_2, up to a fraction of $\sim 10^{-3}$ by number, and the enhanced cooling found by Peebles & Dicke (1968) led to fragmentation of a small fraction of the cloud mass, and to collapse into stars mostly of high mass.

The initial suggestions by Saslaw & Zipoy (1967) and Peebles & Dicke (1968) paved the route to more refined calculations of the role of H_2 formation and cooling in collapsing and fragmenting primordial clouds, mainly with the goal of constraining the typical masses of the forming objects in pregalactic gas clouds (e.g., Hirasawa, Aizu & Taketani 1969; Takeda, Sato & Matsuda 1969; Yoneyama 1970; Hutchins 1976; Silk 1977; Carlberg 1981). The general result was that even a relatively minor fraction of H_2 contributes significant cooling via rotational and vibrational transitions. However, owing to the lack of dipole moment, H_2 molecules have large radiative lifetimes, thus are poor radiators. Nevertheless, these initial calculations showed that during collapse the gas temperature could be kept from climbing above ~ 1000 K over a large density range. As a result, the Jeans mass dropped by many decades and the minimum mass varied between ~ 20 $M_\odot$ and ~ 250 $M_\odot$ with a maximum fractional abundance of H_2 of about 10^{-3} before the onset of collisional dissociation.

The inclusion in the chemical network of three body reactions

$$H + H + H \rightarrow H_2 + H \tag{5}$$

and

$$H + H + H_2 \rightarrow H_2 + H_2. \tag{6}$$

modified this picture considerably (Palla, Salpeter & Stahler 1983). It was found that, over a wide range of initial conditions, virtually all the gas can be converted to molecular form by densities of the order of 10^{12} cm^{-3}. As a result of significant cooling from the molecules, the temperature rise during collapse is slowed and the Jeans mass eventually drops below 0.1 $M_\odot$, thus allowing the formation of low-mass stars even in clouds of primordial composition.

Much of the subsequent effort in the field of primordial chemistry was dedicated to elucidating the atomic and molecular processes, other than those related to H_2, that are important in the early universe after the recombination epoch and prior to first structure formation and reionization. Major studies on this subject include: Lepp & Shull (1984), Black (1990), Puy et al. (1993), Stancil, Lepp & Dalgarno (1996, 1998), Galli & Palla (1998, 2000, 2002), Puy & Signore (2002, 2007), Lepp, Stancil & Dalgarno (2002), Glover & Abel (2008), Schleicher et al. (2008), Glover & Savin (2009), Vonlanthen et al. (2009), and Gay et al. (2011).

3 THE INGREDIENTS OF PRIMORDIAL CHEMISTRY

3.1 Cosmological Model

Over the last few decades, the so-called Λ–Cold Dark Matter (ΛCDM) model has emerged as the standard description of cosmology. Accordingly, the universe is spatially flat, homogeneous, and isotropic on large scales with a scale invariant spectrum of primordial seed perturbations composed of ordinary matter, non-baryonic dark matter and dark energy. The accurate measurements of the peaks in the power spectrum of the CMB, along with baryon acoustic oscillations, the precise estimate of the Hubble constant, of light element abundances

Table 1: Cosmological parameters

Parameter	Value
H_0	$100\,h$ km s^{-1} Mpc^{-1}
h	0.704
$z_{\rm eq}$	3141
$z_{\rm ion}$	10.6
T_0	2.725 K
$\Omega_{\rm dm}$	0.228
$\Omega_{\rm b}$	0.0455
$\Omega_{\rm m}$	$\Omega_{\rm dm} + \Omega_{\rm b}$
$\Omega_{\rm r}$	$\Omega_m/(1 + z_{\rm eq})$
Ω_Λ	0.727
$\Omega_{\rm K}$	$1 - \Omega_{\rm r} - \Omega_{\rm m} - \Omega_\Lambda$
$f_{\rm H}$	0.924
$f_{\rm He}$	0.076
$f_{\rm D}$	2.38×10^{-5}
$f_{\rm Li}$	4.04×10^{-10}

in distant quasars, and the amplitude of mass fluctuations inferred from clusters and gravitational lensing have enabled a deeper and more precise understanding of cosmology (e.g., Spergel et al. 2003; Komatsu et al. 2011). The essential parameters (primary and inferred) of such a precision model are listed in Table 3.1. All the values have been taken from the *WMAP* seven-year mean (cf. Table 1 of Komatsu et al. 2011) with the exception of the current temperature of the CMB from Fixsen (2009), and the element abundances from Iocco et al. (2009). In the Table, $z_{\rm eq}$ represents the redshift of equal energy density between matter and radiation, while $z_{\rm ion}$ is the redshift of reionization on the assumption that the universe was re-ionized instantaneously. The fractional abundances of H, He, D and Li relative to the total number of baryons are given by f(H), f(He), etc.. These cosmological parameters will be adopted in the rest of the discussion and will provide the initial values for the chemical evolutionary models that will be described in the next Section. It is expected that the *Planck* satellite by ESA with higher resolution, sensitivity, and frequency coverage than predecessors will provide an update on the current cosmological parameter estimates as early as 2013.

3.2 Standard Big Bang Nucleosynthesis

According to ΛCDM cosmology, the formation of the first elements occurs entirely during the radiation-dominated epoch at a time $t \sim (T/{\rm MeV})^{-2}$ s, where T is the plasma temperature. This energy scale corresponds to a time scale of a few minutes, temperature of $\sim 10^9$ K, and redshift of $z \approx 10^8$–10^9. The hot and low-density plasma was primarily composed of free nucleons and electrons that initiated the production of light elements (e.g., Fields 2011). Owing to the low density, most of the reactions occur by neutron and proton capture, whereas three body reactions are effectively suppressed, as well as reactions with nuclei heavier than $Z_i Z_j \gtrsim 6$. Thus, at temperatures $T \sim 100$ keV, deuterium (with binding energy 2.2 MeV) can be synthesized via $p(n,\gamma)D$ reactions, since

Table 2: Predicted Abundances from standard BBN

Light Element	PArthENoPE	THALYS
$Y_{\rm pi}$	0.2467	0.2476
D/H ($\times 10^{-5}$)	2.56	2.59
^{3}He/H ($\times 10^{-5}$)	1.02	1.04
^{7}Li/H ($\times 10^{-10}$)	4.60	5.24
^{6}Li/H ($\times 10^{-14}$)	1.11	1.23

blackbody photons can no longer equilibrate the reverse reaction. The abundance of deuterium rises sharply, as almost all available neutrons are locked into D-nuclei. The actual abundance is set by the value of the baryon-to-photon ratio, parametrized by the quantity

$$\eta \equiv \frac{n_{\rm b}}{n_\gamma} = 2.74 \times 10^{-8}\, \Omega_{\rm b} h^2 \tag{7}$$

where $\Omega_{\rm b} = \rho_{\rm b}/\rho_{\rm cr}$, $\rho_{\rm b}$ is the baryon density, $\rho_{\rm cr}$ is the critical density defined by

$$\rho_{\rm cr} = \frac{3H_0^2}{8\pi G}, \tag{8}$$

and h is the present-day value of the Hubble constant measured in units of 100 km s^{-1} Mpc^{-1}. In the following, we will adopt $\eta_{10} = 10^{-10}\eta$.

The WMAP determination of $\eta_{10} = 6.16 \pm 0.15$ implies that the standard BBN has no free parameter left and can yield precise predictions of the abundances of D, ^{3}He, ^{4}He, and ^{7}Li (Serpico, Esposito & Iocco 2004; Iocco et al. 2009; Coc et al. 2012). These abundances can then be used as the initial conditions for the modeling of the chemical evolution of the expanding universe. Table 2 reports the values of BBN calculations obtained with two numerical codes: PArthENoPE (Iocco et al. 2009; Pisanti 2012, priv. comm.), and the nuclear reaction code THALYS (Coc et al. 2012). Although the codes can solve the synthesis of heavy elements (including CNO, ^{9}Be, and B), in the following we only consider the production of light elements since their abundance is sufficient for the chemistry calculations[3]. The predictions of the detailed models of BBN can be compared with the observations of light elements at high z. The literature on this subject is quite extensive and here we briefly summarize the current status (for a review, see, e.g., Steigman 2007).

3.2.1 Deuterium. As for deuterium, there is consistency between the inferred primordial abundance deduced from the angular power spectrum of the CMB, and the predictions of BBN. Assuming that the measured D-abundance in low-metallicity environments at redshifts $z \gtrsim 2$–3 corresponds to the true D/H ratio produced by the BBN (see, e.g., Kirkman et al. 2003), observations of DI and HI absorption lines in damped Ly-α (DLA) systems towards QSOs have provided the best determinations of deuterium. The mean value derived from 8

[3]However, the accurate assessment of the predicted abundances of CNO are of particular relevance for the evolution of Population III stars whose properties are significantly affected for values higher than $\sim 10^{-10}$ in mass fraction (Cassisi & Castellani 1993), or higher than 10^{-12} for low-mass primordial stars (Ekström et al. 2010). This is still at least three orders of magnitude above the yields computed by Coc et al. (2012) and Iocco et al. (2009).

QSO absorbers is (Fumagalli, O'Meara & Prochaska 2011)

$$\log\left(\mathrm{D/H}\right)_{\mathrm{p}} = (2.78 \pm 0.21) \times 10^{-5}. \quad (9)$$

This implies a value of $\Omega_{\mathrm{b}}h^2$ (BBN)= 0.0213 ± 0.0012, in agreement within the errors with the value of $\Omega_{\mathrm{b}}h^2 = 0.0222 \pm 0.0004$ deduced from the angular power spectrum of the CMB (Keisler, Reichardt & Aird 2011). However, the authors note that the scatter between different measurements is larger than the published errors. The preferred explanation of the dispersion is an underestimate of the systematic errors affecting D/H measurements (e.g., Pettini et al. 2008)[4]. Recently, Pettini & Cooke (2012) have obtained an accurate measurement towards the metal-poor ($Z \simeq 10^{-2}\, Z_{\odot}$), DLA at redshift $z = 3.05$ in the $z_{\mathrm{em}} \simeq 3.03$ QSO SDSS J1419+0829 with $\left(\mathrm{D/H}\right)_{\mathrm{p}} = (2.535 \pm 0.05) \times 10^{-5}$ which implies $\Omega_{\mathrm{b}}\, h^2$ (BBN)= 0.0213 ± 0.0012. Similarly, Noterdaeme et al. (2012) have derived a primordial abundance of $\left(\mathrm{D/H}\right)_{\mathrm{p}} = 2.8^{+0.8}_{-0.6} \times 10^{-5}$, consistent with the predictions of BBN using the constraint on $\Omega_{\mathrm{b}}h^2$ from WMAP7.

3.2.2 Helium. The situation for helium is less favorable[5]. Since ^{4}He is produced in stars, the determination of its primordial value requires extrapolation from the measured abundances in metal-poor galaxies (extragalactic HII regions), a procedure which is affected by systematic uncertainties (e.g., Olive & Skillman 2004, Izotov & Thuan 2010). Different analyses have yielded values that differ systematically from each other, with a weighted mean of

$$Y_{\mathrm{p}} = 0.2566 \pm 0.0023, \quad (10)$$

(Aver, Olive & Skillman 2010), that shows a slight discrepancy with the predicted BBN value reported in Table 2. We note that helium has the most accurately predicted abundances and it is quite insensitive to the precise value of the baryon density $\Omega_{\mathrm{b}}\, h^2$. In a recent re-analysis of the dataset of Izotov, Thuan & Stasinska (2007), Aver, Olive & Skillman (2012) using Markov Chain Monte Carlo techniques have obtained an extrapolated primordial value of $Y_{\mathrm{p}} = 0.2534 \pm 0.0083$, in agreement with the WMAP7 result of 0.2487 ± 0.0002.

3.2.3 Lithium. Finally, of all the light elements, lithium (in both isotopic versions, ^{7}Li and ^{6}Li) is most problematic, owing to the well established discrepancy between the predicted abundance of ^{7}Li and the value measured in metal-poor halo dwarf stars. In fact, the observations extended over a time span of about 30 years have confirmed the existence of a discrepancy between the measured value of ^{7}Li/H= $(1.58 \pm 0.31) \times 10^{-10}$ – the so-called Spite plateau – and that inferred from WMAP measurements, larger by a factor of ~ 3 (Iocco et al. 2009). The realization of a dramatic scatter of the ^{7}Li abundance at very low metallicities, below [Fe/H] ≈ -2.8, has complicated the interpretation of the evolution of lithium in low-mass stars even further (see Sbordone et al. 2010 and Bonifacio, Sbordone & Caffau 2012 for a recent analysis). A surprising, yet very encouraging, result has been reported by Howk et al. (2012) who have measured the ^{7}Li abundance in the interstellar medium of the Small Magellanic Cloud. Unlike the

[4] Alternative interpretations involving an early destruction of deuterium have been suggested (Olive et al. 2012).

[5] Since ^{3}He is both produced and destroyed in stars and since it can be observed only in the ISM of the Milky Way (e.g., Bania, Rood & Balser 2010), its abundance is affected by large uncertainties and cannot be used as a test for BBN predictions.

case for old metal-poor stars, the derived abundance of ^{7}Li/H= $(4.8\pm1.7)\times10^{-10}$ is almost equal to the BBN predictions, thus providing a precious hint that the "lithium problem" posed by stellar measurements may not be representative of the primordial value. Since inferring the Li abundance in the ISM in not straightforward and requires several assumptions, these initial results must be substantiated by further analysis.

BBN predicts that ^{7}Li must be definitely more abundant than its isotopic version ^{6}Li by several orders of magnitude (cf. Table 2). High resolution observations of halo stars have been able to detect ^{6}Li with ratios as high as ~ 0.5 (Asplund et al. 2006; García Pérez et al. 2009). However, the observations remain controversial, as well as the evidence for a tendency of ^{6}Li to follow the same Spite plateau. Note that the observations towards the Small Magellanic Cloud give a limit to the isotopic ratio of $^6\mathrm{Li}/^7\mathrm{Li} < 0.28$ (Howk et al. 2012).

The standard BBN model rests on the assumption of homogeneity and isotropy of all constituent species, a hypothesis supported by the observed low amplitude of the CMB temperature fluctuations. However, alternative models of *inhomogeneous* nucleosynthesis have been developed, mainly in order to provide a solution to the ^{7}Li problem. In this case, the the baryon-to-photon and the neutron-to-proton ratios are allowed to vary on small scales allowing for a large variation of the element abundances (see, e.g., Iocco et al. 2009 for a general discussion). Here, it suffices to underline the potential impact that these models have on the yields of CNO and heavier elements as a distinctive diagnostic between standard and inhomogeneous models. Vonlanthen et al. (2009) have investigated the effects of the higher CNO abundances resulting from non-standard BBN and their implications on molecule formation.

3.3 Cosmological Recombination

The importance of cosmological recombination for studies of primordial chemistry and structure formation was already emphasized in the seminal works of Peebles (1968) and Peebles & Dicke (1968). According to Peebles (1968), "one also would like to know the residual ionization in the matter, because the electrons and ions mediate the formation of molecular hydrogen and so help determine the rate of energy radiation by clouds that formed at the Jeans limit". **Figure 1** shows the cosmological recombination of H, D, He and Li. Of all the nuclei of interest, Li^{3+} is the first to recombine at redshift $z \approx 14,000$,

$$\mathrm{Li}^{3+} + e \rightarrow \mathrm{Li}^{2+} + h\nu, \tag{11}$$

then Li^{2+} recombines at $z \approx 8600$,

$$\mathrm{Li}^{2+} + e \rightarrow \mathrm{Li}^{+} + h\nu, \tag{12}$$

followed by the recombination of He^{2+} at $z \approx 6000$,

$$\mathrm{He}^{2+} + e \rightarrow \mathrm{He}^{+} + h\nu, \tag{13}$$

and of He^{+}at $z \approx 2500$,

$$\mathrm{He}^{+} + e \rightarrow \mathrm{He} + h\nu, \tag{14}$$

By $z \approx 2000$ all these reactions have run to completion, owing to the high density of the matter and the large availability of electrons as long as H is still ionized.

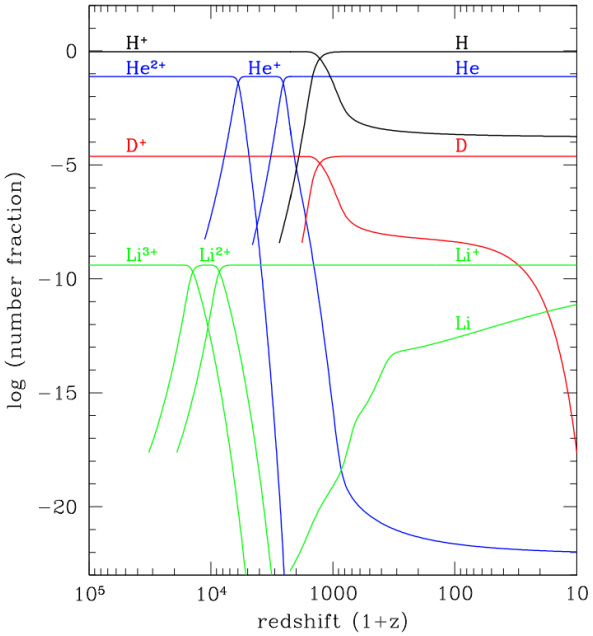

Figure 1: Cosmological recombination of H, D, He, and Li. Note the small residual fraction of H^+ (and He^+), while D^+ is completely removed at low redshifts by charge exchange with H. Unlike all other elements, lithium remains largely ionized even at the lowest redshifts.

Finally, at $z \approx 1300$ hydrogen recombines, along with deuterium:

$$H^+ + e \rightarrow H + h\nu. \tag{15}$$

Notice that the cosmological recombination of Li,

$$Li^+ + e \rightarrow Li + h\nu, \tag{16}$$

essentially never occurs, owing to the photoionization of Li due to ultraviolet photons produced by the recombination of H and He (Switzer & Hirata 2005) and the five orders of magnitude drop of electron abundance following H recombination. Notice also that the residual fraction of D^+, unlike those of H^+ and He^+, does not reach a freeze-out because D^+ is efficiently removed at low redshift by the near-resonant charge-transfer reaction

$$D^+ + H \rightarrow D + H^+, \tag{17}$$

which is exothermic by 3.7 meV (43 K).

3.3.1 Recombination of Hydrogen. The basic physics of cosmological H recombination was fully understood in the late 1960s (Peebles 1968; Zel'dovich et al. 1968; see Peebles 1993). Direct recombination to the $n = 1$ ground state of H or He produces photons which can easily ionize neighboring neutral atoms, because the primordial gas has a large optical depth ($\sim 10^7$) to ionizing photons. Therefore, cosmological H and He recombination proceeds by capture of electrons into excited $n \geq 2$ states followed by decay to the ground state. However, electrons in excited states cannot cascade instantaneously down to the ground state,

because of the large reservoir of photons in the CMB with energies sufficient to produce reionizations out of these states ($E > 3.4$ eV). In fact, the population of these excited states is, with good approximation, in thermal equilibrium with the CMB. In addition, transitions to the ground state produce Lyman photons that can excite other neutral atoms allowing them to be easily re-ionized. Unlike the present-day ISM, where Lyman photons are eventually absorbed by dust, the only way they can escape reabsorption in the conditions of the early universe is through two processes of low efficiency: by redshifting out of the line because of the cosmological expansion, or by two-photon forbidden emission from the $n = 2$ level. The "bottleneck" caused by slow decay from the $n = 2$ to the $n = 1$ level, combined with the density drop due to the expansion, prevents H recombination from being completed and results in a residual fraction of electrons and protons. On the basis of a simple two-level approximation ($n = 1$, $n \geq 2$) plus continuum, Peebles (1968) and Zel'dovich et al. (1968) found a residual ionization 2×10^{-5}–2×10^{-4} depending on the present-day value of the mass density, in agreement with previous estimates of Novikov & Zel'dovich (1967). Many refinements and additional effects were later added to the original formulation (e.g. Matsuda, Sato & Takeda 1971; Jones & Wise 1985; Krolik 1990; Sasaki & Takahara 1993) without however changing the basic concepts summarized above. Still in 2000, the major uncertainty on the residual electron fraction was due to the poor knowledge of the cosmological parameters $\Omega_{\rm b}$ and h.

As a result of the exquisite accuracy of experiments such as WMAP, several detailed multilevel calculations, supplemented by computer codes, are now available to determine with precision better than 0.1% the evolution of the electron fraction down to $z \approx 500$: RECFAST[6] (Seager, Sasselov & Scott 1999,2000; updated by Wong, Moss & Scott 2008 and Scott & Moss 2009); RICO[7] (Fendt et al. 2009); COSMOREC[8] (Switzer & Hirata 2008ab; Ali-Haimoud & Hirata 2010; Chluba, Vasil & Dursi 2010; Grin & Hirata 2010; Rubiño-Martín et al. 2010; Chluba & Thomas 2011); HyRec[9] (Ali-Haïmoud & Hirata 2011); ATLANT[10] (Kholupenko et al. 2011).

3.3.2 Recombination of Helium. Cosmological He recombination was first computed by Matsuda, Sato & Takeda (1969). An updated and detailed review of the processes involved can be found in Switzer & Hirata (2008a,b,c) and Chluba, Fung & Switzer (2012). In currently available computer codes like RECFAST, H and He recombinations are computed simultaneously, with He^+ and He^{2+} treated as multilevel atoms. The recombination of He^{2+} presents no $n = 2$ "bottleneck" because of the high two-photon decay rate. Consequently, the abundance of He^{2+} is well approximated by the Saha formula. This is not true for He^+ recombination, which follows essentially a hydrogenic-like case B recombination and is found to be slow essentially for the same reasons that H recombination is slow (see, e.g., Seager, Sasselov & Scott 2000).

3.3.3 Recombination of Lithium. The calculation of Li recombination has not been straightforward. It was first computed by Palla, Galli & Silk (1995), and later refined by Stancil, Lepp & Dalgarno (1996), Bougleux & Galli (1997)

[6] http://www.astro.ubc.ca/people/scott/recfast.html
[7] http://cosmos.astro.uiuc.edu/rico
[8] http://www.cita.utoronto.ca/∼jchluba/ *Science*_Jens/Recombination/CosmoRec.html
[9] http://tapir.caltech.edu/∼yacine/hyrec/hyrec.html
[10] http://www.ioffe.ru/astro/QC/CMBR/atlant/atlant.html

and Galli & Palla (1998). Defining the recombination redshift $z_{\rm rec,Li}$ as the redshift when $\mathrm{Li}/(\mathrm{Li}+\mathrm{Li}^+) = 0.1$, Stancil, Lepp & Dalgarno (1996) and Galli & Palla (1998) found $z_{\rm rec,Li} \approx 400$–$450$, and a residual Li ionization fraction $\mathrm{Li}^+/\mathrm{Li} \approx 0.5$–$0.7$ as $z \to 0$. However, it was later realized by Switzer & Hirata (2005) that the recombination history of Li is strongly affected by UV photons generated by the recombination of H and He at $z < 1000$ via Ly-α and two-photon decay (see Section 3.3.1). These nonthermal photons are sufficient to reduce the neutral Li fraction by about 3 orders of magnitude at $z = 100$. The resulting evolution with redshift in Figure 1 shows that Li never recombines completely and Li^+ is still $\sim 98\%$ of the total Li at $z = 10$ (cf. Table 4.1). As discussed in Section 6.1, the recombination history of Li has important cosmological consequences.

4 CHEMICAL EVOLUTION AFTER RECOMBINATION

The full network of chemical reactions for the early universe has become increasingly complex over the last decade, from the ~ 90 reactions of Galli & Palla (1998) to the ~ 250 reactions of Gay et al. (2011). The number of species formed from nuclei up to Li is limited to ~ 30, but for state-resolved chemistry each state must be considered as a separate species. Thus, for example, H_2^+ and H_2 require 19 and 15 coupled equations, respectively, one for each vibrational state of the fundamental electronic level (Coppola et al. 2011). The network has been extended to molecular species produced by elements heavier than Li, like F (Puy et al. 2007) and C, N, O (Vonlanthen et al. 2009), but their abundances are extremely small even if non-standard BBN models are adopted. Ignoring the very small change in particle number due to chemical reactions, the total baryon density $n_{\rm b}$ evolves with redshift as

$$n_{\rm b} = \frac{\Omega_{\rm b}\rho_{\rm cr}}{\mu m_{\rm H}}(1+z)^3 \tag{18}$$

where $\rho_{\rm cr}$ is the critical density defined by equation (8), $m_{\rm H}$ is the mass of the hydrogen atom, and $\mu = 4/(4-3Y_{\rm p})$ the mean atomic weight of the primordial gas. Numerically, $n_{\rm b} \approx 2.2 \times 10^{-7}(1+z)^3$ cm^{-3}.

Once formed, molecules can be photodissociated by the CMB photons with rates that depend on its spectrum, a blackbody characterized by a radiation temperature $T_{\rm r} = T_0(1+z)$, with $T_0 = 2.725$ K (see Table 3.1). In addition, distortions of the CMB produced by photons emitted during the recombination of H and He cannot be neglected, as they affect significantly, and in some cases dramatically, the rates of several photodestruction processes, such as H^- photodetachment (see Section 4.1) and Li recombination (see Section 3.3.3).

For applications to the homogeneous universe, the chemical reaction network must be supplemented by a routine that provides the ionization fraction as function of redshift for the adopted cosmological model, and an equation for the evolution of gas temperature $T_{\rm g}$,

$$\frac{dT_{\rm g}}{dt} = -2T_{\rm g}\frac{\dot{R}}{R} + \frac{2}{3kn_{\rm b}}[(\Gamma-\Lambda)_{\rm Compton} + (\Gamma-\Lambda)_{\rm mol} + \Gamma_{\rm chem}]. \tag{19}$$

In this equation, the first term represents the adiabatic cooling of the gas due to the expansion of the universe, R being the scale factor; the second and the third the net transfer of energy (heating Γ minus cooling Λ) from the radiation to the

gas via Compton scattering of CMB photons on electrons, and via excitation and de-excitation of molecular transitions, respectively; the fourth term represents chemical heating of the gas (see e.g. Glassgold, Galli & Padovani 2012). The ionization fraction is sufficient to maintain $T_{\rm g} \approx T_{\rm r}$ up to $z \approx 300$ via Compton heating of the gas. Because of the small molecular abundances, the term $(\Gamma - \Lambda)_{\rm mol}$ is very small and can raise the gas temperature by only a few degrees (Khersonskii 1986; Galli & Palla 1989; Puy et al. 1993). The chemical heating term $\Gamma_{\rm chem}$ is also negligible (Puy et al. 1993). Consequently, at redshift $z \lesssim 100$, the gas cools almost adiabatically, with $T_{\rm g} \approx 0.02(1+z)^2$ K. Additional sources of heating for the gas that could affect its chemical evolution are dark matter particles decays and annihilations (Ripamonti, Mapelli & Ferrara 2007) and ambipolar diffusion of a cosmological magnetic field (Schleicher et al. 2009).

Finally, the chemical network is completed by the equation for the redshift,

$$\frac{dt}{dz} = -\frac{1}{(1+z)H(z)}, \tag{20}$$

where $H(z)$ is the Hubble parameter

$$H(z) = H_0[\Omega_{\rm r}(1+z)^4 + \Omega_{\rm m}(1+z)^3 + \Omega_{\rm K}(1+z)^2 + \Omega_\Lambda]^{1/2}. \tag{21}$$

The meaning of these quantities has been discussed in Section 3.1 and their numerical values are listed in Table 3.1.

4.1 Overview of Global Trends

The evolution of the main molecular species using the cosmological parameters and initial element abundance described before is displayed in **Figure 2** as fractional abundances relative to the total number of baryons. It can be conveniently described following the five main periods during which some common process can be identified that dominates the chemical kinetics of the gas. As a function of decreasing redshift, the sequence is as follows:

I. $2000 \lesssim z \lesssim 800$. At $z \sim 1000$ the ionization fraction is still $\sim 10\%$, while at $z = 800$ it drops to $\sim 1\%$. While hydrogen is still mostly ionized, the availability of protons promotes the initial steep rise of all molecular species. The first reaction to occur is the radiative association of H^+ and He

$$H^+ + He \rightarrow HeH^+ + h\nu, \tag{22}$$

quickly followed by the sequence of radiative association of H and H^+ (reaction 1) that leads to H_2 formation via charge exchange (reaction 2). The formation of H_2^+ via reaction (1) is more efficient than the conversion of HeH^+ to H_2^+ by reaction with hydrogen atoms. In this phase, the main destruction process is through energetic photons from the CMB. As shown in Figure 2, the formation of H_2, HD, H_3^+, and H_2D^+ proceeds quite rapidly and then levels off at a redshift of $z \sim 1000$. However, the HeH^+, H_2^+, and HD^+ abundances display a turnover followed by a decrease to a minimum at $z \approx 800$ due to recombination with electrons.

II. $800 \lesssim z \lesssim 300$. As the ionization fraction freezes out, all the molecular species start forming at a moderate pace, sustained by the decreased importance of photodissociation processes by the CMB. The major limiting factor to

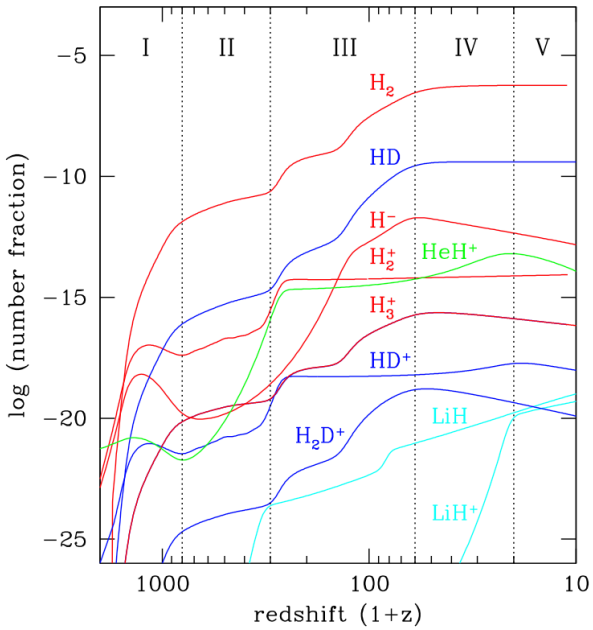

Figure 2: Fractional abundances (relative to the total number of baryons) of the main molecules and ions formed in the early universe as function of redshift. The vertical dotted lines indicate the boundaries of the five main evolutionary phases described in the text.

the increase of H_2 molecules is the importance of deviations from local thermodynamic equilibrium (LTE) in the H_2^+ level population and the highly efficient photodissociation by CMB photons (Hirata & Padmanabhan 2006; Coppola et al. 2011). Thus, the behavior of HD, H_3^+, and H_2D^+ follows exactly that of the H_2 molecules. In principle, the kinetics of HeH^+ formation should also be followed including the effects of non-LTE analysis of the level populations, but this calculation has not been done yet. One would then expect that the steep rise shown in Figure 2 could just reflect the assumption of a LTE level population and that the actual abundance should be considerably reduced. At redshifts $z \lesssim 400$, LiH begins to form by radiative association, but its growth is limited by efficient photodestruction.

III. $300 \lesssim z \lesssim 60$. The abundance of most species rises and reaches a peak value at $z \sim 60$. As the energy density of the CMB photons keeps decreasing, H_2^+ forms more effectively through radiative association of H and H^+, but the charge exchange reaction 2 limits its abundance. At redshifts below ~ 100, the formation of H^- ions starts becoming important as the main route for H_2 formation. H^- ions (binding energy 0.754 eV) are no longer effectively photodetached by the CMB and promote the formation of H_2 molecules by radiative attachment (reaction 4). However, as first computed by Hirata & Padmanabhan (2006), the presence of a significant tail of non-thermal photons of the CMB produced by hydrogen and helium recombination slows down the rise of H^- abundance and, hence, of H_2 and H_3^+.

IV. $60 \lesssim z \lesssim 20$. The abundance of H_2 and HD reaches freeze-out, while that of H^- steadily drops due to its conversion into H_2 molecules. Freeze-out

Table 3: Elemental and molecular abundances relative to hydrogen at $z = 10$

H_2/H	H^-/H	H_2^+/H	H_3^+/H	H_3^-/H	
6.3×10^{-7}	1.8×10^{-13}	9.2×10^{-15}	8.0×10^{-17}	5.5×10^{-33}	
HD/H	HD^+/H	D^+/H	H_2D^+/H		
4.2×10^{-10}	1.2×10^{-18}	6.1×10^{-19}	1.6×10^{-20}		
HeH^+/H	He^+/H	He_2^+/H			
1.7×10^{-14}	9.8×10^{-23}	9.3×10^{-36}			
Li^+/H	Li/H	LiH/H	LiH^+/H	Li^-/H	$LiHe^+/H$
4.3×10^{-10}	8.0×10^{-12}	9.0×10^{-20}	4.6×10^{-20}	1.7×10^{-22}	3.0×10^{-23}

is achieved when the formation time becomes longer then the Hubble expansion time. At redshift $z \lesssim 40$ the marked increase in the HeH^+ and HD^+ abundance results from the exponential drop in the reaction

$$HeH^+ + H \rightarrow He + H_2^+ \tag{23}$$

below $T_g = 100$ K (Bovino et al. 2011c). Some of the HeH^+ participates in the enhanced formation of HD^+ via

$$HeH^+ + D \rightarrow HD^+ + H, \tag{24}$$

which drives further production of H_2^+ and HD^+. Below $z \approx 40$, LiH^+ is readily formed due to the decrease of the intensity of the CMB, and its abundance reaches that of LiH.

V. $z \lesssim 20$. As first structure formation begins to be important, the steady decrease of some species is accounted for by the relevant role played by dissociative recombinations. Interestingly, only H_2 and HD have reached their steady state abundances, whereas the rest remain out of equilibrium. This fact introduces some arbitrariness in the initial conditions for the calculations of the dynamical evolution of the density perturbations, even though the minute fractional abundances of most chemical species do not affect the thermal properties of the primordial gas.

The chemical evolution of each element will now be described in some detail.

4.2 The Chemistry of Hydrogen

4.2.1 H_2 FORMATION THROUGH EXCITED STATES. During the recombination era, the formation of H_2 molecules can proceed either via radiative association of excited hydrogen atoms (Latter & Black 1991)

$$H(n = 2) + H(n = 1) \rightarrow H_2(X\,^1\Sigma_g^+) + h\nu \tag{25}$$

or via Raman association (the inverse Solomon process; Dalgarno & van der Loo 2006; Alizadeh & Hirata 2011)

$$H + H + h\nu \rightarrow H_2(B\,^1\Sigma_u^+, C\,^1\Pi_u) \rightarrow H_2(X\,^1\Sigma_g^+) + h\nu, \tag{26}$$

where $X\,^1\Sigma_g^+$ is the ground state of H_2, and $B\,^1\Sigma_u^+$ and $C\,^1\Pi_u$ are the excited electronic states with energies $\sim$10 eV. The potential curves of the $B\,^1\Sigma_u^+$ and

$C\,^1\Pi_u$ with allowed transitions to the $X\,^1\Sigma_g^+$ ground state of H_2 correlate with atomic hydrogen in $n = 2$ (both $2s$ and $2p$) and $n = 1$ levels, respectively.

In the first process, as pointed out by Latter & Black (1991), the population of the $n = 2$ excited level is maintained over the LTE value as a result of resonant scattering by Ly-α photons (Peebles 1968; Zel'dovich et al. 1968), thus allowing reaction (25) to occur rapidly at a typical rate of few 10^{-14} cm^3 s^{-1} over a temperature interval of 50–30000 K. Latter & Black showed a pronounced increase of H_2 molecules due to this reaction in the redshift interval between 2500 and 1500.

Recombination of H_2 by Raman association is facilitated owing to the abundance of ultraviolet photons, both blackbody CMB photons (Dalgarno & van der Loo 2006) and spectral distortion photons (Alizadeh & Hirata 2011). The resulting excited H_2 molecule reemits the photon and can decay either to the bound state $X\,^1\Sigma_g^+$ or to the continuum of the X level leading to dissociation. Dalgarno & van der Loo (2006) computed the H_2 production rates via Raman association including all relevant rovibrational resonances and found them to be more dominant than the radiative association channel of reaction (25). In these calculations, most of the contribution to H_2 formation occurs at a redshift $z \approx 1600$.

On the other hand, Alizadeh & Hirata (2011) have demonstrate the importance of the distortion photons of the CMB using a code that included the absorption and emission of Lyman-series photons in the HI lines. This contribution starts to be dominant at redshifts $z \lesssim 1400$ when the photon density deviates significantly from the Planck spectrum. The overall effect is a *net* reduction of the H_2 abundance due to efficiency of the inverse of reaction (25). In the redshift interval 1300–900, the H_2 fractional abundance remains well below the value of 10^{-16}, several orders of magnitude lower than the value computed neglecting this process. At lower redshifts, however, the process becomes rapidly negligible as the spectral distortion is redshifted at energies lower than the Lyman-Werner bands. Interestingly, Alizadeh & Hirata (2011) find that the H_2 abundance is too low to affect the recombination process or to introduce secondary anisotropies in the CMB: in principle, absorption or emission of H_2 molecules of photons above the Lyman-Werner bands could add or remove photons that would otherwise excite a hydrogen atom and alter the recombination history.

4.2.2 State-resolved formation of H_2 and H_2^+. At redshifts lower than $z \approx 800$, the abundance of H_2 molecules is determined by the balance between charge transfer with H_2^+ ions, reaction (2) and the reverse of reaction (1). Other minor routes involve reactions of HD molecules with either H or H^+. In spite of its simplicity, the kinetics of the main reactions for H_2 is quite complex due to the presence of a large number of quantum states and the evaluation of the exact vibrational distribution function is indeed necessary (see, e.g., Lepp, Stancil & Dalgarno 2002). This aspect has proved particularly important in the case of the photodissociation rates of H_2^+ ions, the main destruction route in competition with conversion into H_2 molecules, which have usually been computed either assuming LTE level populations of the rovibrational levels or with all the H_2^+ ions in the ground state. Detailed calculations of the fully level-resolved populations of H_2^+ have been performed by Hirata & Padmanabhan (2006) and Coppola et al. (2011; see also Longo et al. 2011). The resulting behavior is shown in **Figure 3a**. The main conclusion of these studies is that full thermalization of the vibrational levels is never achieved since the vibrational relaxation processes

are too slow to balance the strong vibrational selectivity of formation rates and radiative processes affect both the vibrational distribution function and the overall fractional abundances. As a consequence of the non-LTE level population, the formation of H_2 molecules is greatly reduced mainly because the H_2^+ ions are photodissociated before they can either decay to the ground state or undergo charge transfer to become H_2 molecules.

4.2.3 H_2 FORMATION VIA H^- IONS. The last step in the formation of H_2 molecules is via associative detachment, reaction (4). Recently, the cross section for this simple reaction has been accurately measured in experiments with merged beams apparatus at collision energies of cosmological interest (Kreckel et al. 2010; Miller et al. 2011). Once formed, H^- ions are readily destroyed by photons of the CMB owing to the rather low photodetachment threshold energy (0.754 eV). The major improvement on the precise magnitude of this process has been the inclusion of the spectral distortions in the CMB (Hirata & Padmanabhan 2006). The rate coefficient for photodetachment can be written as

$$k_{\rm nonth} = n_{\rm H} c \int_{\nu_0}^{\infty} r_\nu \sigma_\nu \frac{d\nu}{\nu} \tag{27}$$

where r_ν is the number of recombination photons per H atom and per logarithmic frequency range, σ_ν is the photodetachment cross section and $h\nu_0 = 0.754$ eV. The nonthermal photons become the dominant process at redshifts below $z \approx 130$ when the photon energy is ~ 1 eV, corresponding to the peak of the photodetachment cross section. The effect on the H^- abundance is clearly visible in **Figure 3b** where the sharp peak at $z \approx 100$ (dotted line) is replaced by a shallow increase and a maximum at $z \approx 60$. This behavior accounts for the evolution of H_2 molecules, also shown in Figure 3b. Unlike the case without non-thermal photons, the fractional abundance of H_2 reaches the freeze-out value only at $z \lesssim 60$, when the nonthermal photons have been redshifted below the threshold. The freeze-out value of H_2 molecules at $z = 10$ is 6×10^{-7}.

4.2.4 MINOR SPECIES: H^-, H_2^+ AND H_3^+. As shown in Figure 3b and Table 4.1, the fractional abundance of these species at $z = 10$ is very small, varying between $\sim 10^{-13}$ for H^- and $\sim 10^{-16}$ for H_3^+. The reason why H^- ions do not reach equilibrium at the lowest redshifts is that they are constantly removed by the radiative association with H atoms to form H_2 molecules. Similarly, the H_3^+ ion displays a steady decrease from its peak abundance of $\sim 2.5 \times 10^{-16}$ at $z \approx 50$ due to efficient destruction by dissociative recombination with electrons. According to the experimental results of McCall et al. (2004) and Kreckel et al. (2005), the dissociative reaction rate is in general agreement with the theoretical predictions and the branching ratios tend to favor the channel H+H+H over the H+H_2 channel. The global evolution of H_3^+ follows quite closely that of H_2 as the main formation process is via radiative association with H^+ at all redshifts. Due to its potential importance as a coolant of the collapsing gas, we shall return to H_3^+ in the discussion on the rates (Section 4.6).

As for H_2, the behavior of H_2^+ is strongly affected by the inclusion of the non-LTE level population in the calculation of the photodissociation rate, which is the main destruction process of this ion. The latter ceases to be important at redshifts below $z \approx 300$ and that explains the flattening of the abundance shown in Figure 3a. At lower redshifts, formation by radiative association is balanced by charge exchange reaction into H_2, accounting for a nearly constant fractional

abundance of $\sim 10^{-14}$. Finally, at redshifts smaller than $z \approx 60$, the formation of H_2^+ is enhanced by the HeH^+ channel via the reaction with H_2^+ whose rate drops significantly at temperatures below $T_g \approx 100$ K (Bovino et al. 2011c), as will be discussed in Section 4.4.

We also mention the possibility of the formation of H_3^-, the negatively charged counterpart of H_3^+, which is predicted to be stable by about 0.013 eV (Stärck & Meyer 1993). Recently, Ayouz et al. (2011) have developed the theory of its formation in the ISM by radiative association of H_2 and H^- and derived the relevant cross sections. Using the reaction rate by Ayouz et al. (2011), we have verified that the resulting abundance is negligible ($\lesssim 10^{-30}$) at all redshifts.

4.3 The Chemistry of Deuterium

Deuterium in the early universe is important for a variety of reasons. First, owing to its larger mass, deuterated hydrogen has a spacing of the rotational levels smaller than that of hydrogen molecules. Thus, cooling through HD dipole radiation can effectively drive the primordial gas to substantially low temperatures, provided a sufficient abundance is obtained. Thus, the chemistry of deuterium has been computed by numerous groups following the initial study of Lepp & Shull (1984), such as Dalgarno & Lepp (1987), Latter (1989), Puy et al. (1993), Palla, Galli & Silk (1995), Stancil, Lepp & Dalgarno (1998), Galli & Palla (1998, 2002), Lepp, Stancil & Dalgarno (2002), and Glover & Abel (2008). Recently, Gay et al. (2011) have presented a thorough analysis of the chemistry of highly deuterated species, including D_2, D_2^+, D_2H^+, and D_3^+. The formation of HD follows two main routes involving a deuteron exchange with H_2

$$D + H_2 \rightarrow HD + H, \tag{28}$$

and

$$D^+ + H_2 \rightarrow HD + H^+. \tag{29}$$

The thermal rate constant for reaction (28) has been measured in numerous experiments over a wide range of temperatures (e.g., Mitchell & LeRoy 1973; Michael & Fisher 1990); theoretical calculations (e.g., Mielke et al. 1994; Charutz, Last & Baer 1997) show very good agreement with each other and with the experimental data. Reaction (29) represents the major source of HD in diffuse interstellar clouds (Dalgarno, Weisheit & Black 1973). Its rate coefficient is almost constant and close to the Langevin value 2.1×10^{-9} cm^3 s^{-1} (e.g., Gerlich 1982). Finally, at $z \lesssim 10$, HD formation takes place via charge exchange (Karpas, Anicich & Huntress 1979)

$$HD^+ + H \rightarrow HD + H^+. \tag{30}$$

The destruction of HD occurs mainly via the reverse reactions of (28) and (29)

$$HD + H \rightarrow D + H_2 \tag{31}$$

and

$$HD + H^+ \rightarrow D^+ + H_2. \tag{32}$$

The rate coefficient for the first reaction has been computed by Shavitt (1959) using a semi-empirical H_3 energy surface. As for reaction (32), owing to its endothermicity by 0.0398 eV (462 K), the removal of HD at low temperatures is reduced by a factor $\exp(-462\ \mathrm{K}/T_g)$, leading to significant fractionation. At

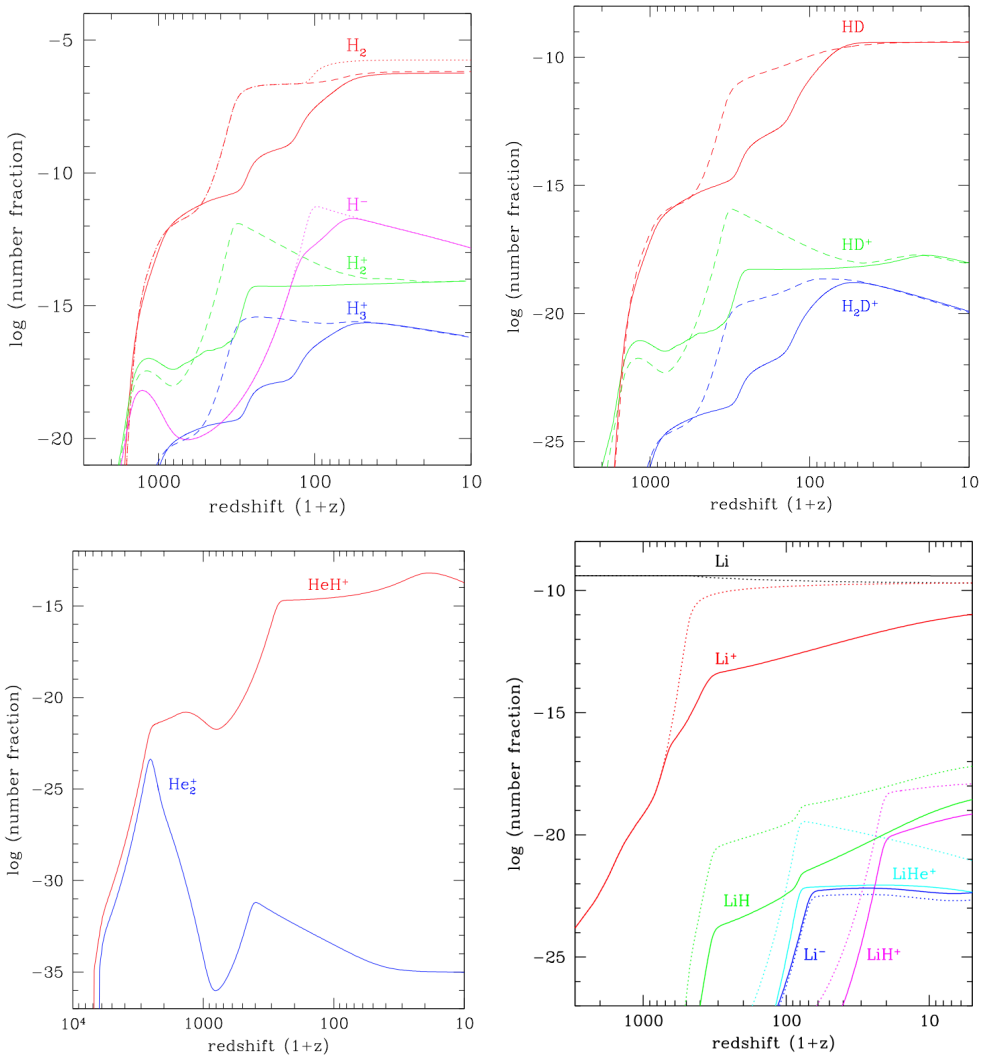

Figure 3: (*a*) Hydrogen chemistry. The solid curves show the case with state-resolved formation of H_2 and H_2^+, while the dashed lines correspond to the evolution obtained by ignoring this effect. The dotted lines display the evolution of H_2 and H^- without the contribution of the non-thermal photons of the CMB to the photodissociation of H^-. (Adapted from Coppola et al. 2011). (*b*) Deuterium chemistry. The solid and dashed curves have the same meaning as in the caseAstron. Astrophys. of the hydrogen chemistry shown in Figure 3a. (Adapted from Galli & Palla 2002). (*c*) Helium chemistry. Evolution of the main He-bearing molecular ions, HeH^+ and He_2^+. (Adapted from Bovino et al. 2011c). (*d*) Lithium chemistry. Evolution of Li-bearing molecules and ions with (solid curves) and without (dotted curves) the effects of non-thermal photons on Li recombination. In the latter case, Li never recombines, molecular abundances decrease significantly at all redshifts, with the exception of Li^-, and LiH remains the most abundant species. (Adapted from Bovino, Tacconi & Gianturco 2011b and Bovino et al. 2011d).

freeze-out, the ratio $HD/H_2 \approx 7 \times 10^{-4}$, with an enhancement factor of ~ 25 over the initial D/H abundance.

The relative abundance of D and D^+, is governed by the charge exchange reactions

$$H^+ + D \rightarrow H + D^+, \tag{33}$$

and

$$H + D^+ \rightarrow H^+ + D. \tag{34}$$

Since reaction (33) has a threshold of 43 K, the rate coefficient for reaction (34) is usually obtained by multiplying that of reaction (33) by $\exp(43\ \mathrm{K}/\mathrm{T_g})$. Savin (2002) has computed accurate rate coefficients for both reactions, improving on the early estimates by Watson (1976) and Watson, Christensen & Deissler (1978) that have been widely used in studies of deuterium chemistry.

Figure 3b highlights the close similarity of the evolution with redshift of the HD abundance with that of H_2 and the dramatic effect of including the state resolved levels in the calculations. Generally, the chemistry of HD is dominated by the ion-neutral reactions (29) and (32) in a gas of low density (e.g., prior to the formation of the first structures), whereas the neutral-neutral reactions (28) and (31) become more important in conditions of high density and temperature (as during cloud collapse or in shocked gas).

Figure 3b also displays the evolution of the main deuterated cations HD^+ and H_2D^+. The case of H_2D^+ is of interest due to the suggestion of Dubrovich (1993) and Dubrovich & Lipovka (1995) that its abundance could reach significant values (up to $H_2D^+/H_2 = 10^{-5}$), in which case specific rovibrational transitions could leave detectable imprints on the spectrum of the CMB. In principle, such an abundance could result from the complete conversion of H_3^+ into H_2D^+ following deuterium fractionation at low temperatures ($T_g \ll 50$ K). However, the actual abundance of H_3^+ in the primordial gas is quite low due to fast dissociative recombination. Although Dubrovich & Lipovka (1995) claim observable features in the CMB for abundances of H_2D^+ as low as 10^{-8}, Figure 3b shows that this value is never achieved in the post-recombination universe where H_2D^+ reaches a peak of only $\sim 2 \times 10^{-19}$ at $z \sim 80$. On the other hand, the isotopic ratio is enhanced with respect to the primordial D/H abundance by a factor of ~ 8. As in the case of H_3^+, the main removal of H_2D^+ occurs via dissociative recombination.

Finally, the chemistry of HD^+ is directly related to that of H_2^+ since its abundance is determined by the equilibrium between the forward and reverse reaction

$$H_2^+ + D \rightarrow HD^+ + H. \tag{35}$$

HD^+ would maintain the freeze-out value of $\sim 5 \times 10^{-19}$, reached at a redshift of ~ 250 if not for the enhancement due to the production from HeH^+ via

$$HeH^+ + D \rightarrow HD^+ + He. \tag{36}$$

Comparison of Figure 3a and Figure 3b visualizes the similar behavior of HD^+ and H_2^+, as well as H_2D^+ and H_3^+.

4.4 The Chemistry of Helium

The helium hydride ion (HeH^+) and the molecular helium ion (He_2^+) contend for the role of the first molecular species formed in the universe. Searches for

HeH^+ in space, either in gaseous nebulae (Moorhead et al. 1988, Liu et al. 1997, Dinerstein & Geballe 2001) or in high-redshift absorbers (Zinchenko, Dubrovich & Henkel 2011), have only given tentative detections.

In the early universe, HeH^+ and He_2^+ are formed at $z \approx 7000$ by radiative association of He with H^+ and He^+, respectively. The rate of the former process is well determined theoretically (Saha, Datta & Barua 1978; Flower & Roueff 1979; Roberge & Dalgarno 1982; Basu & Barua 1984; Kimura et al. 1993; Dumitriu & Saenz 2009; Sodoga et al. 2009) and the absolute photodissociation cross section has been measured by the free electron laser FLASH (Pedersen et al. 2007), although at high photon energy (38.7 eV). Some studies have also addressed the enhancement of the photodissociation rate produced by CMB photons (Juřek, Špirko & Kraemer 1995; Zygelman, Stancil & Dalgarno 1998). The rate of the He_2^+ formation has a temperature dependence similar to that of the radiative association of H and H^+, but is about one order of magnitude smaller (Stancil, Babb & Dalgarno 1993).

The history of helium chemistry is displayed in **Figure 3c**. Since He^+ recombines rapidly at $z \approx 2500$, the abundance of He_2^+ reaches a maximum of $\sim 10^{-23}$ around this redshfit, and then is readily destroyed by photodissociation and dissociative recombination. In contrast, the incomplete recombination of H^+ keeps the abundance of HeH^+ steadily rising to $\sim 10^{-13}$ at $z \approx 20$. The main reactions responsible for the bumpy behavior of the evolution of HeH^+ and that limit its final abundance are photodissociation for $z \gtrsim 300$, collisions with H for $20 \lesssim z \lesssim 300$ (Linder, Janev & Botero 1995, Bovino et al. 2011c), and dissociative recombination for $z \lesssim 20$ (Guberman 1994). As mentioned in Section 4.2, destruction of HeH^+ by collisions with H atoms is an important source of H_2^+ and accounts for its enhancement at the smallest redshifts. Finally, at redshifts below $z \approx 800$, photodissociation processes become inefficient, and the abundance of He_2^+ rises again by about 5 orders of magnitudes, but its growth is limited by efficient destruction by collisions with H for $z \lesssim 400$.

In spite of the potential importance of HeH^+ molecules for efficiently scattering the CMB photons (see Section 6), an accurate calculation of photodissociation rates is still lacking. Miyake, Gay & Stancil (2011) have obtained cross sections for all rotational transitions from the vibrational levels $v'' = 0$–11 of the $^1X\Sigma^+$ state for temperatures between 500 and 12,000 K, including both $X \leftarrow X$ and $A \leftarrow X$ transitions. These cross sections can then be used to directly obtain the photodissociation rate due to the CMB radiation. Miyake et al. present some initial estimate for different radiation temperatures and find that at redshifts $\gtrsim 1000$ the $A \leftarrow X$ transitions (which are usually neglected) dominate the photodissociation, while at lower redshifts the $X \leftarrow X$ transition become more important. Thus, one would expect that the initial rapid rise of the HeH^+ abundance shown in Figure 3c will be further reduced by inclusion of this photodestruction channel. Future work is needed in order to clarify the magnitude of this effect.

4.5 The Chemistry of Lithium

The chemistry of lithium in the early universe has been reviewed by Dalgarno, Kirby & Stancil (1996), Stancil, Lepp & Dalgarno (1996), Bougleux & Galli (1997), Galli & Palla (1998), Puy & Signore (2002) and Bodo, Gianturco & Martinazzo (2003). After the recombination of Li^{3+} and Li^{2+} (see Section 3.3), the main remaining species Li and Li^+ react with the residual electrons, H, D, and

He atoms and ions to form Li^-, LiH, LiH^+, LiD, LiD^+, $LiHe^+$ and Li^-. The chemical network of lithium is complex (for updated chemical reaction rates see Bovino, Stoecklin & Gianturco 2010; Bovino et al. 2010; Bovino, Tacconi & Gianturco 2011b; Bovino et al. 2011d; Bovino et al. 2012), but the molecular abundances are very small. In addition, as these species are easily photodissociated, their formation in significant amounts is delayed to relatively low redshifts, $z \lesssim 200$. To complicate matters, the evolution is also extremely sensitive to the effects of nonthermal photons from the recombination of H and He (cf. Switzer & Hirata 2005). The latter can easily maintain Li ionized down to the lowest redshifts, whereas in their absence lithium would recombine at the same level of Li^+. This behavior is displayed in **Figure 3d** where the dramatic effect of the inclusion of non-thermal photons can be appreciated by comparing the evolution in the two cases. In addition to the neutral and singly ionized species, some Li^- ions can also form at redshifts below $z \sim 100$. Their evolution follows closely that of H^-, both anions being removed at low temperatures mainly by reactions of mutual neutralization with H^+, with a rate typically proportional to $T_g^{-1/2}$. As a result, the abundance of Li^- at $z = 10$ is $\sim 2 \times 10^{-22}$.

The first Li-bearing molecule to form is LiH mainly via radiative association,

$$\mathrm{Li} + \mathrm{H} \rightarrow \mathrm{LiH} + h\nu, \tag{37}$$

with a contribution for $20 \lesssim z \lesssim 80$ from Li^- via the reaction

$$\mathrm{Li}^- + \mathrm{H} \rightarrow \mathrm{LiH} + e. \tag{38}$$

Note, however, that the rate for the latter reaction is only estimated. Radiative association takes place first from the $\mathrm{Li}(^2P)$ state, then from the $\mathrm{Li}(^2S)$ state. Since the ^2P level lies about 1.85 eV above the ^2S level, the formation of LiH molecules via electronically excited levels is important only at $z \gtrsim 800$, when the temperature is greater than some thousand degrees K. Early estimates for the radiative association rate from the ^2S state resulted in relatively large values, and therefore the abundance of LiH in the early universe was expected to be a substantial fraction of the Li abundance (Lepp & Shull 1984). However, the situation was clarified by refined quantum mechanical calculations that reduced significantly the magnitude of the cross sections (Dalgarno, Kirby & Stancil 1996; Gianturco & Gori Giorgi 1996). As for destruction, LiH is easily photodissociated by CMB photons for $z \gtrsim 300$, whereas at lower redshifts it is mainly destroyed by collisions with H, a process for which quantal calculations are available (Bovino, Wernli & Gianturco 2009).

Owing to the small binding energy (0.14 eV), the main production of LiH^+ via radiative association of Li with H^+ is delayed until redshifts below $z \approx 40$, although a minute contribution can result at $z \gtrsim 700$ from reactions of Li^+ ions with H. The reaction rates for both channels have been computed with fully quantal methods (Dalgarno, Kirby & Stancil 1996; Gianturco & Gori Giorgi 1997). As in the case of LiH, photodissociation is the dominant destruction mechanism of the molecular ion, with an uncertain contribution from collisions with H and a contribution from dissociative recombination (Čurik & Greene 2007,2008) at very low redshifts ($z \lesssim 20$). Interestingly, at $z = 10$ the abundance ratio of LiH/LiH^+ is ~ 2, either including or ignoring the non-thermal photons of the CMB.

Finally, $LiHe^+$ is formed by spontaneous and stimulated radiative association of Li^+ with He (Bovino, Tacconi & Gianturco 2011a, 2012). At $z \gtrsim 100$, $LiHe^+$ is

destroyed by photodissociation, while at lower redshift by collisions with H and by dissociative recombination (Bovino et al. 2012). However, the abundance of $LiHe^+$ at $z = 10$ remains exceedingly small, $\sim 4 \times 10^{-23}$.

4.6 Critical Rates

As stressed in the Introduction, the evolution described so far depends more on the uncertainties of the chemical model than on the initial conditions provided by the cosmological models. The abundances of the various species are only as accurate as the rates given as input. The literature is rich in studies that critically examine the uncertainties of the reaction rates and their effects on the chemistry (and cooling) of the primordial gas. Most of the important reactions involved in the chemistry of the major species have well determined rate coefficients. Below, we give a brief overview of the rates for the most relevant reactions or that still present significant differences either from theory or from experiments. Extensive and updated compilations of reaction rates can be found in Glover & Abel (2008), Schleicher et al. (2008), Glover & Savin (2009), Bovino et al. (2011d), and Gay et al. (2011).

4.6.1 Associative detachment of H^-. Surprisingly enough, in spite of many years of research, there has been considerable uncertainty on both the magnitude and temperature dependence of the rate of this important reaction that affected all the calculations of the chemical and thermodynamical evolution of Population III stars (e.g., Glover, Savin & Jappsen 2006). The series of merged beams measurements carried out by Bruhns et al. (2010), Kreckel et al. (2010), Miller et al. (2011) and the ion trap study by Gerlich et al. (2012) have given results in agreement with the theoretical predictions (e.g., Sakimoto 1989, Cízek, Horácek & Domcke 1998). **Figure 4** illustrates the good match (to within $\pm 25\%$) between experimental data of Gerlich et al. (squares), Bruhns et al. (solid line) and theory (dashed curve) over a wide temperature interval and highlights the departure from the Langevin value that had been previously adopted in chemical models. The impact of the newly computed rates on the collapse and fragmentation of primordial clouds has been discussed by Kreckel et al. (2010) who have shown that the uncertainty on the predicted Jeans mass of the fragments is reduced from a factor of 20 to only a factor of 2 (see Savin et al. 2012; Savin 2013).

4.6.2 Mutual neutralization of H^- and H^+. Although this process is irrelevant in the chemistry of the expanding universe, it becomes important when the gas gets reionized and recombines out of equilibrium during the gravitational collapse phase (see, e.g., Glover, Savin & Jappsen 2006). The older experiment by Moseley, Aberth & Peterson (1970) reports cross sections that are consistently higher at energies above 3 eV than the most recent ones by Szucs et al. (1984) and Peart & Hayton (1992). The latter are in very good agreement with the theoretical calculations (see, e.g., Stenrup, Larson & Elander 2009). Experiments at energies below ~ 3 eV are required in order to remove the remaining uncertainty (Urbain et al. 2010).

4.6.3 Radiative association of H_2^+. This reaction which dominates the H_2^+ kinetics is important at all temperatures and redshifts. The rate coefficient calculated by Stancil, Babb & Dalgarno (1993) is in excellent agreement with the older results of Ramaker & Peek (1976). Below ~ 10 K, the rate is basically constant at the value of $\sim 2 \times 10^{-20}$ cm^3 s^{-1} which accounts for the flat portion

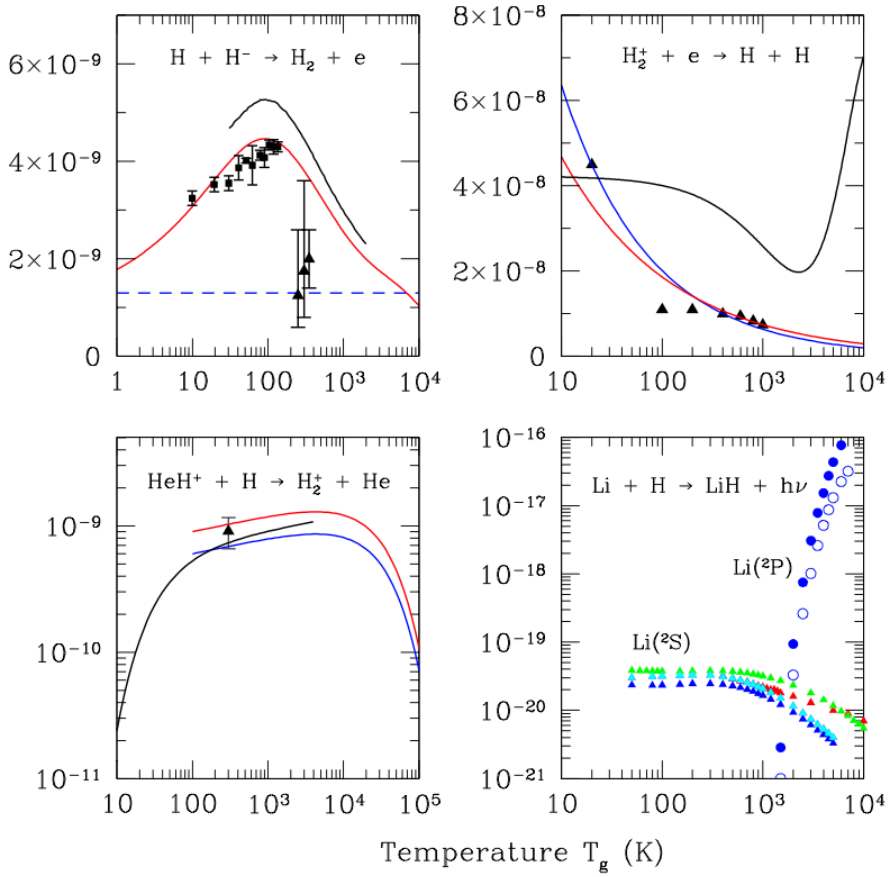

Figure 4: Rate coefficients (in $\mathrm{cm}^3\ \mathrm{s}^{-1}$) for some critical reactions. *Upper left panel:* Filled squares: data from Gerlich et al. (2012) with 1σ statistical uncertainty. Black line: results from the merged-beam experiments of Bruhns et al. (2010) and Miller et al. (2011). Red curve: calculation by Cízek et al. (1998). Triangles: measurements at room temperature by Schmeltekopf, Fehsenfeld & Ferguson (1967), Fehsenfeld, Howard & Ferguson (1973), and Martinez et al. (2009, slightly shifted for better readability). Short-dashed line: Langevin value. *Upper right panel:* Blue and red curves: fits by Galli & Palla (1998) and Stancil, Lepp & Dalgarno (1998) of the rate by Schneider et al. (1994) for the $v = 0, J = 0$–20 levels (triangles). Black curve: LTE rate computed by Coppola et al. (2011) from the state-resolved cross sections of Takagi (2002). *Lower left panel:* Triangle: experimental result at 300 K (Karpas, Anicich & Huntress 1979). Red and blue curves: reaction rate obtained by Stancil, Lepp & Dalgarno (1998) and Schleicher et al. (2008) from the experimental cross sections of Linder, Janev & Botero (1995). Black curve: result of the quantum calculations by Bovino et al. (2011c). *Lower right panel:* Li(^2S): data from Dalgarno, Kirby & Stancil (1996, cyan), Gianturco & Gori Giorgi (1996, blue), Bacchus-Montabonel & Talbi (1999, red), Bennett et al. (2003, 2008, green). Li(^2P): data from Gianturco & Gori Giorgi (1997, blue) for the $B^1\Pi \rightarrow X^1\Sigma^+$ (filled dots) and the $A^1\Sigma^+ \rightarrow X^1\Sigma^+$ (empty dots), respectively.

of the curve of the H_2^+ abundance at low redshifts (see Figure 3a). We note that the fitting formulae given by Stancil, Lepp & Dalgarno (1998) and Gay et al. (2011) become inaccurate below $T_g \sim 10$ K, possibly affecting the resulting H_2^+ abundance at the lowest redshifts.

4.6.4 PHOTODISSOCIATION OF H_2^+. This is the main destruction process for H_2^+ which determines the history of H_2 molecules down to redshifts $z \sim 300$. State-resolved cross sections have been calculated by Dunn (1968), Stancil, Babb & Dalgarno (1993), Lebedev, Presnyakov & Sobel'Man (2000), and Hirata & Padmanabhan (2006). However, only the early results of Dunn (1968) are available in tabular form and have been adopted in the work by Coppola et al. (2011) on which the discussion of Section 4.2 is based.

4.6.5 CHARGE EXCHANGE OF H_2 WITH H^+. This endoergic reaction has a threshold of 1.83 eV. The most complete theoretical work on this chemical reaction is that of Krstić (2002). The thermal rate coefficient has been computed by Savin et al. (2004) for $H_2(v = 0, J = 0)$. Glover & Abel (2008) discuss the large uncertainties on this rate that exist in the literature, quoting as extreme values the prescription by Shapiro & Kang (1987) based on detailed balance from the reverse reaction, and the much lower rate of Abel et al. (1997), based on cross sections by Janev, Langer & Evans (1987). However, the latter is valid only at temperatures higher than $\sim 10^4$ K, and should not be used at lower temperatures where it exponentially drops to unrealistic values. At temperatures above $\sim 10^3$ K, the rate coefficient by Savin et al. (2004) is in excellent agreement with the fit by Galli & Palla (1998) based on cross sections of Holliday, Muckerman & Friedman (1971). At lower temperatures, the exponential drop due to the energy threshold makes the uncertainty in the rate coefficient of no consequence for primordial chemistry and collapse calculations.

4.6.6 CHARGE EXCHANGE OF H_2^+ WITH H. Also for this exoergic reaction, state-resolved cross sections have recently been computed by Krstić (2002) for collision energies in the range 0.6–9.5 eV, but need to be extrapolated to lower energies for applications to primordial chemistry. The extrapolation is usually made in such a way as to reproduce the value of the thermal rate of this reaction measured by Karpas, Anicich & Huntress (1979) at $T_g = 300$ K (Coppola et al. 2011). Clearly, specific calculations at low energy (and additional experimental measurements) are needed.

4.6.7 DISSOCIATIVE RECOMBINATION OF H_2^+. A wealth of theoretical and experimental data is available for the dissociative recombination of H_2^+ and its isotopologues (see, e.g., Schneider & Suzor-Weiner 2002). The level of experimental accuracy made possible by the advent of storage-ring experiments has encouraged a continuous refinement of the computational techniques and the inclusion of previously neglected physical processes. Using multi-quantum defect theory, Takagi (2002) has calculated state-resolved dissociative recombination cross sections that include the rotational structure and all excited dissociative states. A relevant characteristic is the presence of many resonances at low energies, and the sensitivity of the cross section to the vibrational quantum number v, especially at low energies. As a result, the reaction rate computed by Coppola et al. (2012) in LTE has a non-monotonic behavior significantly different from the usual power-law approximations commonly adopted in the literature (see Figure 4).

4.6.8 THREE-BODY H_2 FORMATION. In the low density gas of the expanding universe, three-body reactions cannot take place. However, in the collapsing clouds of the primordial halos where the first generation of stars is thought to occur, these reactions effectively transform the atomic gas into fully molecular hydrogen at densities above $\sim 10^9$ cm^{-3}. In addition, since each reaction liberates 4.48 eV of energy, corresponding to the binding energy of H_2, into the gas, three-body reactions represent an important energy source for the dynamical evolution of the clouds. The main reaction for H_2 formation involves atomic hydrogen as the third body, but a number of other channels are also possible. Although there is consensus on the small value of the rate coefficient of the reaction, the numerical values quoted by different authors vary by up to two orders of magnitude at the low temperatures of interest for cosmological simulations, while there is substantial agreement (to within a factor of $\sim$2) at temperatures greater than $\sim$ 2000 K (see, e.g., Glover & Savin 2009).

Current estimates of the three body reaction rates are based on laboratory measurements of the reverse reaction, collisional dissociation of H_2 by hydrogen atoms, using the principle of detailed balance (e.g., Palla, Salpeter & Stahler 1983; Flower & Harris 2007). Similar, although smaller, differences exist in the rate coefficients for reactions where the third body is an H_2 molecule. The source of the discrepancy is attributed by Flower & Harris (2007) to different assumptions made for the equilibrium constant. However, including the nuclear degeneracy, as well as the electron spin degeneracy, in the calculation removes the discrepancy and reduces the rate to the values adopted by Palla, Salpeter & Stahler (1983) (F. Esposito, priv. comm.). An even lower value of the rate was proposed by Abel et al. (2002), based on the calculations of Orel (1987) at temperatures < 300 K and assuming an inverse temperature dependence at higher temperatures. From the theoretical viewpoint, Esposito & Capitelli (2009) have presented a unifying approach that includes the contributions from quasibound and unbound states by means of the classical orbiting resonance theory (e.g., Orel 1987) and from continuum states through directly calculated dissociation with detailed balance application. Their total recombination rate shows a dependence on the temperature to pressure ratio, but it is in fairly good agreement with the estimates of Abel, Bryan & Norman (2002) at low temperatures.

Performing direct experiments of three-body association has proved extremely difficult in the laboratory due to the high densities and temperatures required. Savin (2013) gives an account of the challenges of such experiments and concludes that the situation is not too promising in the short term. Turk et al. (2011) have performed an analysis of the effects of the current uncertainty in the rate using 3D simulations of the collapse of primordial clouds in the high density regime. The results clearly show how sensitive the outcome is to the precise value and temperature dependence on the rate, concluding that "the uncertainty represents a major limitation on our ability to accurately simulate the formation of the first stars in the universe". Clearly, this is a field that urgently requires some basic technological or methodological breakthrough.

4.6.9 RADIATIVE ASSOCIATION OF H_3^+. Although the reaction

$$H_2 + H^+ \rightarrow H_3^+ + h\nu \tag{39}$$

is the main route for H_3^+ formation, the rate coefficient has an uncertainty of four orders of magnitude. The study of Gerlich & Horning (1992) based on an ion trap measurement and a classical trajectory analysis recommends the constant

value of 1×10^{-16} cm^3 s^{-1}. This value has been adopted in most chemical models (e.g., Schleicher et al. 2008; Glover & Savin 2009). However, Stancil, Lepp & Dalgarno (1998), on the basis of quantal calculation of other diatomic molecules, argue that the rate should be much smaller and indicate a value of 1×10^{-20} cm^3 s^{-1} also adopted in the recent compilation of Gay et al. (2011). The evolution of H_3^+ is clearly affected by such a large uncertainty. If instead of the large rate, the value suggested by Stancil, Lepp & Dalgarno (1998) had been adopted in the chemical model discussed in Section 4.2, the resulting abundance of H_3^+ would decrease by three orders of magnitude with respect to that shown in Figure 3a. Thus, this reaction needs to be further investigated before the effective role of H_3^+ can be elucidated.

4.6.10 Dissociative recombination H_3^+ and H_2D^+. The ion storage ring measurements of McCall et al. (2004) and Kreckel et al. (2005) have settled the issue of the rate coefficient of this most relevant reaction. Previously, a large uncertainty existed between the results of merged beam experiments with typical values of $\sim 10^{-7}$ cm^3 s^{-1} at room temperatures (e.g., Sundström, Mowat & Danared 1994) and of flowing afterglow experiments with values about ten times smaller (e.g., Smith & Španel 1993). More recent experiments (e.g., Glosík et al. 2008), as well as refined theoretical calculations have converged towards the results of McCall et al. (2004) with the remaining disagreement below a factor of 2. In the evolution presented here, we have followed McCall et al. (2004) using a branching ratio of 0.66 for the recombination into H + H + H and of 0.34 into H_2 + H$^+$. As for H_2D^+, the experiments of Datz et al. (1995) and Larsson et al. (1996) still remain the main source for the determination of the rate coefficient with branching ratios of 0.73 for the channel H + H + D, 0.20 for HD + H, and 0.07 for H_2 + D.

4.6.11 Isotopic exchange of HD. In spite of being the most important channel for the destruction of HD, only sparse laboratory data exist for reaction (31). In addition, all the experiments are limited to temperatures greater than $\sim$ 200 K (e.g., Galli & Palla 2002), thus confirming the plea made long ago by Shavitt (1959) for more experimental work on such a basic reaction.

4.6.12 Transfer reaction of HeH$^+$. Reaction (23) is the main destruction channel of HeH$^+$ in the redshift interval $300 \lesssim z \lesssim 10$. Prior to Bovino et al. (2011c), it was not studied with sufficient accuracy from a theoretical point of view. The crossed-beam data for energies higher than 0.2 eV (Rutherford & Vroom 1973) were fitted by Linder, Janev & Botero (1995) and adopted in the chemical models of Schleicher et al. (2008). Bovino et al. (2011c) present new ab initio quantum calculations for this process for collision energies from 10^{-4} eV to 1 eV. The reaction rate is displayed in Figure 4. The marked drop of the thermal rate below $T_g \approx 100$ K is due to the non-Langevin behavior of the cross sections at energies below $\sim 10^{-2}$ eV.

4.6.13 Radiative association of LiH. The cross sections and rates for the radiative association from the Li(^2P) state have been computed by Gianturco & Gori Giorgi (1997). As for the ^2S state, using semi-classical arguments, Lepp & Shull (1984) estimated a radiative association rate $\sim 10^{-17}$ cm^3 s^{-1}, a value confirmed by Khersonskii & Lipovka (1993). Subsequent quantal calculations performed by two groups on the basis of independent sets of potential curves and wavefunctions (Dalgarno, Kirby & Stancil 1996; Gianturco & Gori Giorgi 1996) provided a value of the rate smaller than the previous results by about three orders

of magnitude. Semiclassical calculations by Talbi & Bacchus-Montabonel (1998) and Bacchus-Montabonel & Talbi (1999) were found in agreement with the quantal results. The inclusion of quasi-bound levels with radiative widths exceeding their tunneling widths (Bennett et al. 2003) resulted in an increase of the rate by a factor of ~ 2. The rates of radiative association of LiH from the ^2S and ^2P states are shown in Figure 4 as function of temperature.

5 COOLING OF THE PRIMORDIAL GAS

Cooling and thermal balance of the primordial gas are key ingredients in the formation of the first structures, as they determine the characteristic fragmentation scale of the clouds and the magnitude of the accretion flow onto the growing protostars (e.g., Abel et al 2002; Yoshida et al. 2006). While chemistry determines the abundances of the main molecular constituents of the gas, the microphysics of each individual component defines the cooling efficiency of the gas. In the case of the homogeneous expanding universe, the thermal balance of the gas is simply set by adiabatic expansion since molecules do not form in sufficient fraction to effectively couple the matter and radiation fields (see Section 4). However, in the collapsing gas of the first minihalos or larger halos, the density and temperature increase considerably allowing the excitation of more molecular degrees of freedom. Thus, a detailed knowledge of the main cooling agents is needed to determine the thermal state of the gas.

5.1 Molecular Cooling

In order to evaluate the cooling function at each redshift, the radiative and collisional transition probabilities and the frequencies of the rovibrational transitions must be specified for each molecule. These data can be found in the literature not only for the most relevant molecules, like H_2 and HD, but also for the other species, such as H_2^+, H_3^+, HD^+, H_2D^+, HeH^+, LiH, and LiH^+. Then, for each molecule, one must solve the level populations from the rate equations. The studies by Glover & Abel (2008) and Glover & Savin (2009) provide detailed discussions for each species. More recently, Coppola, Lodi & Tennyson (2011) has computed updated radiative cooling functions valid in the high-density regime where LTE conditions prevail. One should notice that accurate collisional coefficients are available only in limited cases, and for the minor species simple approximations are used in the evaluation of the cooling functions. We summarize in **Figure 5** the individual cooling functions for the most relevant species in the low-density case (a) and in LTE conditions (b), respectively.

5.1.1 H_2 COOLING. In spite of its dominant role, H_2 has two basic limitations: the excited ro- and vibrational transitions have small radiative transition probabilities (radiative lifetimes $\gtrsim 10^6$ s) and collisional deexcitation becomes competitive with spontaneous transitions at rather low densities ($n \sim 10^4$ cm^{-3}). Thus, as the density increase the cooling rate of H_2 reaches the LTE value which depends only on the transition probabilities and the energy levels. Since the former are small, the cooling rate is also small. The second effect is the onset of optical depth in the cores of the rovibrational lines that effectively reduces the cooling efficiency and requires the solution of the appropriate radiative transfer equations. Detailed calculations have shown that the cooling by H_2 molecules is effectively suppressed at densities $n \gtrsim 10^{10}$ cm^{-3} (e.g., Yoshida et al. 2006).

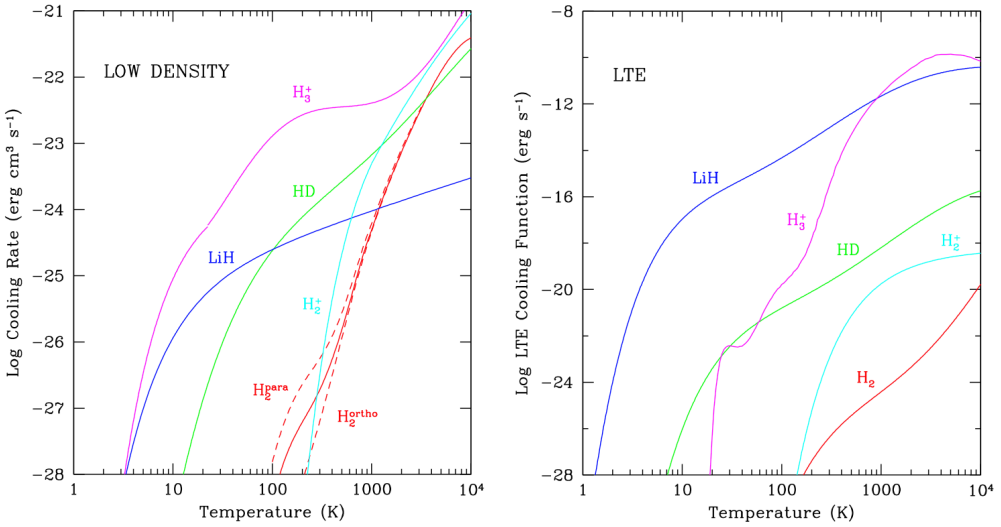

Figure 5: Cooling rate/function for H_2, H_2^+, H_3^+, HD, and LiH in the low-density (*a*) and LTE (*b*) limits. In the low-density case, we plot the cooling rate of ortho-H_2, para-H_2 (dashed curves), and total H_2 (solid curve) assuming an ortho/para ratio of 3:1. Sources for the individual low-density cooling rates are: Glover & Abel (2008) for H_2; Suchkov & Shchekinov (1978) and Glover & Savin (2009) for H_2^+; Glover & Savin (2009) for H_3^+; Lipovka, Núñez-López & Avila-Reese (2005) for HD; Bougleux & Galli (1998) for LiH. Sources for the LTE cooling functions are: Coppola et al. (2012) for H_2; Glover & Abel (2008) for H_2^+; Glover & Savin (2009) for H_3^+; Coppola et al. (2011) for HD and LiH.

Another important aspect is the H_2 ortho/para ratio, since the equilibrium value of 3:1 is achieved only at relatively high temperature and densities. Indeed, in the expanding low-density universe, the H_2 formation process can decrease the LTE value for abundances $f_{H_2} \lesssim 10^{-6}$. Glover & Abel (2008) have shown that for $H^+/H \gtrsim 10^{-4}$ and temperatures lower than several hundred K, the ortho/para ratio is controlled by collisions with protons, so that the cooling rate is mainly due to para-H_2 ($J = 2$–0, $\Delta E/k = 510$ K), although most of the gas contains ortho-H_2 ($J = 3$–1, $\Delta E/k = 845$ K).

In the low-density limit, the total cooling is the sum of individual contributions due to the collisional partners of H_2: H, H_2, He, electrons, and protons. Glover & Abel (2008) provide a thorough discussion and empirical prescriptions of the various terms. Some recent improvements concern the H_2–H_2 collisions, discussed by Lee et al. (2008, see also Balakrishnan et al. 2011) who provide updated collisional coefficients based on the potential energy surface of Diep & Johnson (2000).

5.1.2 HD COOLING. Due to small but non zero dipole moment (8.3×10^{-4} debyes), HD has radiative lifetimes that are a factor of ~ 100 shorter than those of H_2, so that the cooling rate reaches its LTE limit only at densities $n \sim 10^6$ cm^{-3}. In addition, unlike H_2 molecules, transitions with $\Delta J = 1$ are permitted, allowing cooling to occur through the $J = 1$–0 transition (corresponding to $\Delta E/k = 128$ K). Finally, due to the exothermicity of reaction (29) by 462 K, HD is highly fractionated at low temperatures, thus boosting the relevance

of this molecule as an important coolant for the gas at the lowest temperatures. The cooling function computed by Lipovka, Núñez-Lopéz & Avila-Reese (2005) for HD-H collisions for $1 \lesssim n \lesssim 10^8$ cm^{-3} and $100 \lesssim T_{\rm g} \lesssim 10^4$ K, still remains the main reference. In fact, it is in very good agreement with the results of Wrathmall, Gusdorf & Flower (2007) who have improved the interaction potential and included a larger set of rovibrational levels. In the LTE limit, Coppola, Lodi & Tennyson (2011) find a slightly larger (factor of ~ 2) cooling rate for temperatures $T_{\rm g} \gtrsim 700$ K due to the contribution of highly excited rovibrational levels. Collisions of HD with He and electrons have been studied by Nolte et al. (2012) and Yoon et al. (2010), respectively. However, to our knowledge, the corresponding cooling functions have yet to be evaluated.

5.1.3 LiH and LiH^+ cooling. The very large dipole moment (5.89 debyes) of LiH makes this molecules an excellent radiator, and potentially important as a coolant of the primordial gas. However, its low abundance renders its contribution to the total cooling rate insignificant in the expanding universe while it may play a role in collapse calculations. The cooling function for collisions with H has been computed by Bougleux & Galli (1997, fitted by Galli & Palla 1998). These results are valid below a critical density of $n_{\rm cr} \approx 10^{12}$ cm^{-3} (Lepp & Shull 1984), and are still commonly used in the literature. At densities larger than $n_{\rm cr}$, the radiative cooling rate is provided by Coppola, Lodi & Tennyson (2011) who computed updated potential energy and dipole moment curves. As for LiH^+, whose abundance is slightly smaller than that of LiH, only the LTE cooling rate is available (Coppola, Lodi & Tennyson 2011). Its value is a factor of 10–100 smaller than that of LiH, making LiH^+ a negligible coolant in cosmological conditions.

5.1.4 Minor species. Cooling by H_3^+ has been the subject of a detailed analysis by Glover & Savin (2009) and Miller et al. (2010). The former find that H_3^+ is the third important coolant after H_2 and HD in dense ($n \approx 10^7$–10^9 cm^{-3}) primordial gas. In this density regime, the consequences of the large uncertainty on the rate of radiative association of H_3^+ discussed in Section 4.6 are not as strong as those on the expanding medium, because other channels dominate the formation of this ion. As for H_2^+ and HD^+, Glover & Savin (2009) give cooling functions both in the low- and high-density regime. In the latter case, however, Coppola, Lodi & Tennyson (2011) find a HD^+ cooling rate larger by orders of magnitude than that of Glover & Savin (2009) at temperatures $\lesssim 500$ K. Finally, the LTE cooling rate of HeH^+ and its isotopologues has been computed by Coppola, Lodi & Tennyson (2011) (see also Miyake & Stancil 2007). Due to is large dipole moment (1.66 debyes, Pavanello et al. 2005), the LTE cooling rate is estimated to be about ten orders of magnitude grater than that of H_2. No calculations are available for the low-density regime.

5.2 Chemical and Thermal Evolution of Collapsing Primordial Clouds

The well constrained initial conditions provided by the standard ΛCDM model (see Section 3.1) and the knowledge of the atomic and molecular processes in the primordial gas allow the investigation of the evolution of dark matter structure and the formation of the first objects. Current consensus is that the first generation of stars started to take place at redshifts $z \approx 20$–30 in dark matter halos of

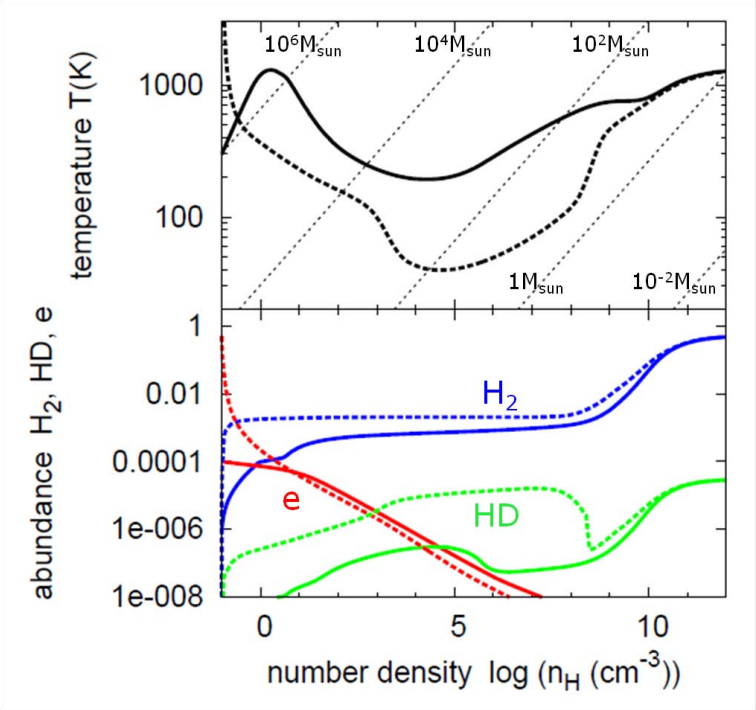

Figure 6: Thermal (*upper*) and chemical (*lower*) evolution of collapsing primordial gas clouds. The solid lines refer to the case of collapse in a predominantly neutral minihalo, while the dashed lines display the evolution of gas which is pre-ionized and cools from high temperatures. Lines of constant Jeans mass are shown as dotted lines in the upper panel. (Courtesy of K. Omukai).

mass $\sim 10^6$ $M_\odot$ (called minihalos) and preceded the formation of the first galaxies (e.g. Bromm 2012). In these minihalos, star formation could proceed thanks to the cooling provided by H_2 molecules (Couchman & Rees 1986; Tegmark et al. 1997) in a predominantly atomic gas and without the complications of physical processes (viz., turbulence, magnetic fields, etc.) that characterize the environment of present-day molecular clouds (however, for a different view see, e.g., Schleicher et al. 2009; Clark et al. 2011; Turk et al. 2012).

Along with the prevailing minihalos, the ΛCDM model predicts the presence of more rare, massive halos with mass $\sim 10^8$ $M_\odot$ and characteristic temperature of $\sim 10^4$ K, too hot for the survival of molecular hydrogen. In this case, it is believed that the gas can cool via atomic hydrogen (Oh & Haiman 2002), but fragmentation is effectively suppressed with the possible formation of massive/supermassive black holes (Bromm & Loeb 2003; Hosokawa et al. 2012). However, a situation in which molecular cooling becomes relevant is when the gas is reionized and recombines out of equilibrium, as in expanding HII regions and intergalactic shocks (e.g. Shapiro & Kang 1987). The resulting enhanced ionization fraction promotes the efficient formation of H_2 via the H^- channel and HD molecules through D^+ via reaction (29). If the HD abundance becomes larger than a critical value, the gas can cool below the floor temperature of ~ 200 K produced by H_2, and even approach the minimum value set by the CMB (Johnson & Bromm 2006; Yoshida, Omukai & Hernquist 2007; McGreer & Bryan 2008).

The thermal and chemical evolution of the collapsing primordial gas can be understood following the results of simplified 1-D calculations that capture the essential microphysics. **Figure 6** illustrates the two cases discussed above: a predominantly neutral medium in a minihalo and a pre-ionized medium.

5.2.1 Formation of first stars in minihalos. As shown in Figure 6 (solid curves), due to the low initial fractional H_2 abundance ($f_{H_2} \lesssim 10^{-6}$), the gas collapses almost adiabatically and H_2 formation proceeds mainly via the H^- channel. At relatively low densities ($n \approx 10$ cm^{-3}), the fractional abundance rises to $f_{H_2} \approx 10^{-3}$ which is sufficient to greatly enhance the cooling efficiency via rovibrational transitions that effectively contrasts the gravitational compression of the gas and produces the marked drop in temperature shown in Figure 6 up to densities $n \approx 10^4$ cm^{-3}. The minimum temperature of ~ 200 K sets a characteristic mass for fragmentation of

$$M_J \approx 1800\,\mathrm{M}_\odot \left(\frac{n}{10^4\ \mathrm{cm}^{-3}}\right)^{-1/2} \left(\frac{T_\mathrm{g}}{200\ \mathrm{K}}\right)^{3/2}. \quad (40)$$

This mass scale is a robust result, rather insensitive to variations in the initial conditions. At higher densities, however, H_2 molecules reach LTE conditions and line cooling saturates. The gas temperature rises slowly with density, while the fractional H_2 and HD abundances remain basically constant at a value of $f_{H_2} \approx 10^{-3}$ and $f_{HD} \approx 10^{-7}$. The major change occurs at densities higher than $\sim 10^8$ cm^{-3} when three body reactions begin to convert the prevailing atomic hydrogen into H_2 molecules, which partly offset the rise in temperature. The increased H_2 abundance drives the accelerated formation of HD molecules. At densities higher than $\sim 10^{12}$ cm $^{-3}$, the cooling is governed by H_2 collision-induced emission and dissociation. Once H_2 molecules are almost completely destroyed, the gas temperature increases adiabatically and pressure forces eventually succeed in effectively halting gravitational collapse and a protostellar core is formed that accretes rapidly matter from the surrounding cloud.

The final outcome of the collapse and the typical masses of the first stars are still subject to uncertainty. While for a certain time it seemed that the first stars were predominantly very massive with characteristic masses $\gtrsim 100$ M$_\odot$ (e.g., Abel et al. 2002; Bromm, Coppi & Larson 2002; Yoshida et al. 2006), more recent calculations including feedback effects have shown that the growth of protostars at the very high accretion rates ($\dot{\mathrm{M}} \gtrsim 10^{-3}$ M$_\odot$ yr^{-1}) expected due to the lack of coolants can be limited to $\lesssim 50$ M$_\odot$ for a wide range of initial conditions (McKee & Tan 2008; Hosokawa et al. 2011). High-resolution 3-D simulations have also shown that multiple fragments can develop during collapse and circumstellar disk formation, thus leading to the formation of binary or small multiple systems or even small clusters of stars of typically low mass (Clark, Glover & Klessen 2008; Clark, Glover & Smith 2011; Turk, Abel & O'Shea 2009; Stacy, Greif & Bromm 2010). Considering the sensitivity of the accretion history on the thermal and dynamical state of the parent gas cloud and on the physical characteristics of the minihalos, it is likely that collapse and fragmentation of the primordial gas will produce a first generation of stars with a substantial distribution in mass.

5.2.2 Formation of stars from pre-ionized gas. The thermo-chemical evolution of primordial gas (see Figure 6, dashed curves) differs significantly from that described above, especially in the initial phases of rapid cooling and enhanced

H_2 formation that results from out-of-equilibrium recombination of electrons with protons. In these conditions, the higher ionization fraction promotes the rapid formation of H_2 molecules that reach fractional abundances of about 5×10^{-3} at densities $\lesssim 1$ cm^{-3}, a factor of $\gtrsim 50$ higher than in the neutral case. As a response, the gas drops to temperatures well below ~ 150 K, the threshold value for HD formation (Omukai et al. 2005). More HD molecules are readily formed, up to $f_{\rm HD} \approx 10^{-5}$, while the gas cools to ~ 30 K at densities $\sim 10^4$ cm^{-3}, so that the characteristic mass given by eq. (40) becomes ~ 100 M$_\odot$. The evolution at higher densities is similar to what described before. The main difference is the predicted lower masses that would result from the fragmentation of primordial gas into smaller clouds of typical solar/subsolar mass (e.g., Nakamura & Umemura 2002; Nagakura & Omukai 2005; Johnson & Bromm 2006).

6 INTERACTIONS OF MOLECULES WITH THE CMB

The study of the interaction of primordial molecules with the CMB is important in view of the possibility to observationally detect spectral distortions or spatial anisotropies imprinted by molecular transitions on CMB photons as they travel from the last scattering surface to a present-day observer. Before the COBE mission (Smoot et al. 1992), much of the interest about primordial molecules as a source of opacity was motivated by the lack of evidence for spatial anisotropies in the CMB, leaving the possibility that an absorbing layer of molecules extending over a significant range of redshifts could smear out any primary anisotropy produced at higher redshift and possibly generate detectable secondary spatial/spectral features (Dubrovich 1977,1994; Maoli, Melchiorri & Tosti 1994; Maoli et al. 1996; Puy & Signore 2002).

Starting from the late 70s, the main effect investigated was resonant scattering by molecules in protogalactic clouds moving at some peculiar velocity with respect to the Hubble flow (Dubrovich 1977), a process analogous to the Thomson scattering of CMB photons by free electrons (Sunyaev & Zel'dovich 1970). Resonant scattering by molecules, like the Sunyaev-Zel'dovich effect, is an elastic process in which a low energy photon ($h\nu \ll m_e c^2$) is absorbed and then re-emitted at the same frequency but in a different direction, isotropically in the rest frame of the absorber but anisotropically in the observer's frame. If the scattering particles have a density $n_{\rm s}$ and a peculiar velocity $v_{\rm pec}$ along the line of sight (positive away from the observer), the induced spectral/spatial anisotropy in the CMB temperature to the lowest order in $v_{\rm pec}/c$ is

$$\frac{\Delta T_{\rm r}}{T_{\rm r}} = -\frac{v_{\rm pec}}{c}(1 - e^{-\tau_\nu}) \tag{41}$$

where

$$\tau_\nu = \int n_{\rm s} \sigma_\nu \, d\ell, \tag{42}$$

is the optical depth of the protogalactic cloud. For free electrons, σ_ν is independent of frequency and equal to the Thomson cross section $\sigma_{\rm T} = 8\pi e^4/(3m_e^2 c^4)$, whereas for electrons bound in molecules the scattering is frequency-dependent and resonant at the frequency of a molecular transition: for a single transition with frequency ν_{ul} between two levels with density populations $n_{\rm l}$, $n_{\rm ui}$, statistical

weights g_l, g_u and Einstein coefficient A_ul, the absorption cross section is

$$\sigma_\nu = \frac{c^2}{8\pi\nu^2} A_\mathrm{ul} \left(1 - \frac{g_\mathrm{l} n_\mathrm{u}}{g_\mathrm{u} n_\mathrm{l}}\right) \frac{g_\mathrm{u}}{g_\mathrm{l}} \phi(\nu - \nu_\mathrm{ul}) \tag{43}$$

where $\phi(\nu - \nu_\mathrm{ul})$ is the line profile. The important fact here is that the absorption cross section of electrons bound in molecules is several orders of magnitude larger than the Thomson cross section of free electrons. Resonant scattering can also be greatly enhanced by luminescence, i.e. the absorption of a high energy photon corresponding to a rovibrational transition followed by the re-emission of several lower energy photons (Dubrovich & Lipovka 1995). Since at $z \approx 300$–500 the frequencies of rotational transitions fall in the Rayleigh-Jeans region of the CMB whereas the frequencies of rovibrational transitions fall around the peak, where the photon density is maximum, luminescence can result in an increase of $\Delta T_\mathrm{r}/T_\mathrm{r}$ at low frequencies by orders of magnitudes for molecules possessing low-energy rotational transitions like LiH and H_2D^+ (Dubrovich 1997).

The limits of integrations in equation (42) depend on the size of the proto-galactic cloud where molecules are located. In the case of a uniform distribution of molecules in the primordial gas, with the abundance depending on redshift as described in the previous sections, is convenient to transform the integration over space in an integration over redshift, $d\ell = c\, dz/H(z)$, where $H(z)$ is the Hubble parameter defined by equation (21). In practice, the absorption (or emission) of photons observed today with frequency ν occurs in a small range of redshifts $\Delta z_\mathrm{i} \approx (1 + z_\mathrm{i})\Delta\nu_\mathrm{th}/\nu_\mathrm{ul}$ around the interaction redshift z_i defined by the condition $\nu(1 + z_\mathrm{i}) = \nu_\mathrm{ul}$. Since spectral lines expected to arise in the dark ages are narrow ($\Delta\nu_\mathrm{th}/\nu_\mathrm{ul} \ll 1$), the region contributing to the optical depth is also small ($\Delta z_\mathrm{i}/z_\mathrm{i} \ll 1$) and can be approximated by a Dirac delta in evaluating the integral in equation (42) (for details, see e.g. Bougleux & Galli 1997).

6.1 Optical Depth

In a cold gas made mainly of H and He very few atomic transitions can be excited at low temperatures. A notable exception is the hyperfine 21 cm transition of neutral hydrogen, with an energy difference between the $F = 1$ and $F = 0$ levels corresponding to 0.068 K. This spin-flip transition is expected to have resonantly absorbed CMB photons in the post-recombination era, producing a broad absorption feature at frequencies of ~ 10 MHz (Varshalovich & Khersonskii 1977, see also Field 1959). However, the detection of this feature is severely hindered, at least from the ground, by ionospheric distortion and reflection of radio waves and by the Galactic synchrotron emission that dominates the CMB by several orders of magnitude in this frequency range (Jester & Falcke 2009). The sensitivity of this transition to a variety of processes that can affect the temperature evolution of the gas before and during reionization, when the 21 cm signal (either in absorption or in emission) is redshifted to more convenient frequency bands around ~ 100 MHz, has made this line a prime target for the new generation of radio interferometers like LOFAR and SKA (for a recent review of 21 cm line cosmology, see Pritchard & Loeb 2012).

In addition to the 21 cm line of neutral H, the 6708 Å resonance transition between the ground state ^2S and the first excited state ^2P of neutral Li can also provide a source of opacity of the primordial gas, as first proposed by Loeb (2001). Stancil et al. (2002) found that this process could result in a possibly detectable

suppression of the power spectrum amplitude of the CMB. However they did not consider the dramatic impact of non-thermal photons on the recombination history of Li, as discussed in Section lithiumrecombination. When this effect is taken into account, the abundance of neutral Li decreases by orders of magnitude, and the optical depth of the Li 6708 Å line is reduced to only a few 10^{-5} (Switzer & Hirata 2005).

Unlike atoms, molecules possess rovibrational transitions that can be excited at the low temperatures characteristic of the pregalactic gas. Early calculations of the contribution of primordial molecules to the opacity of the universe were heavily affected by large uncertainties on the fractional abundance of the species considered. Dubrovich (1977) computed the optical depth of the lowest rotational transitions of HD^+, LiH, para- and ortho-H_2D^+ and found that the latter could reach unity at cm wavelengths if $H_2D^+/H \approx 10^{-6}$. Special attention was given to LiH, because of its high dipole moment (5.89 debyes, Wharton, Gold & Klemperer 1960), and therefore its strong rotational and rovibrational transitions (see, e.g., Zemke & Stwalley 1980; Bellini et al. 1994; Gianturco et al. 1996). In addition, because of the lack of accurate quantal rates for the radiative association of LiH, during the 1980s and early 1990s the conversion of Li into LiH was expected to be almost complete, as described in Section 4.5.

Recently, Black (2006) has computed the opacity associated with bound-free photodetachment transitions of the negative hydrogen ion H^- on the CMB, and found an optical depth of more than 10^{-5} at mm wavelengths, which would have observable effects on the CMB. Following Black's suggestion, Schleicher et al. (2008) analyzed both the bound-free and the free-free absorption of H^-, including the corrections for stimulated and spontaneous emission, and found that the optical depth is dominated by the free-free process for frequencies below $\sim$ 100 GHz, with a ν^{-2} frequency dependence, and by the bound-free process at higher frequencies. The value of the optical depth however is only $\sim 10^{-9}$ at mm wavelengths, much lower than the estimate by Black (2006). In any case, the negative hydrogen ion remains the main source of opacity in the dark ages at frequencies below $\sim$ 30 GHz, whereas at higher frequencies the optical depth is dominated by the contribution of rotational transitions of HeH^+ and the ^2S–^2P transition of Li.

Figure 7 shows the optical depth as function of frequency of H (21 cm line), Li (6708 Å line), H^-, HeH^+, HD^+, LiH and H_2D^+, computed with the abundances shown in Figures 3a–d. From lower to higher frequencies, the optical depth is dominated by pure rotational transitions and rovibrational transitions (free-free and bound-free transitions, respectively, in the case of H^-). For LiH and H_2D^+ only the contribution of pure rotational transitions is present in this range of frequencies.

6.2 Spectral Distortions

Besides the smallness of the optical depth of the main molecular species, another limitation to the detection of spectral distortions in the CMB induced by resonant molecular scattering is the low value of the peculiar velocity $v_{\rm pec}$ with respect to the sound speed. The magnitude of the peculiar velocity has a maximum value of $\sim$ 900 km s^{-1} for protogalactic clouds of masses 10^9–10^{11} M$_\odot$ and is lower for larger or smaller masses (see e.g. Maoli et al. 1996). It also decreases with redshift as $(1+z)^{-1/2}$. Thus, $v_{\rm pec}/c \lesssim 10^{-3}/(1+z)^{1/2}$. Contributions to $v_{\rm pec}$ can

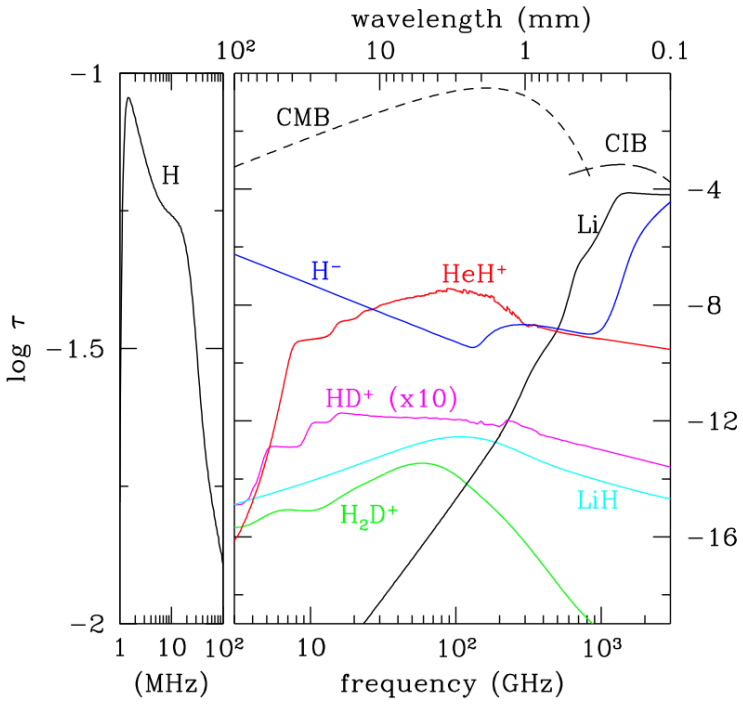

Figure 7: Redshift-integrated optical depth for several primordial atoms, molecules and ions as function of frequency/wavelength. For clarity, the optical depth due to the 21 cm line of neutral hydrogen is shown on a separate panel, and the contribution of HD^+ has been displaced upwards by a factor of 10. For comparison, the intensity of the CMB and the Cosmic Infrared Backround (CIB) are also shown in arbitrary units. Details of the calculations for each species can be found in Palla, Galli & Silk (1995), Bougleux & Galli (1997), Palla & Galli (2000), Switzer & Hirata (2005), Schleicher et al. (2008).

also come from internal hydrodynamical flows, like gravitational collapse. The maximum collapse velocity is in this case of the order of the free-fall speed, or about 100–300 km s^{-1} in the same mass range. Finally, the observation of spectral distortions induced by resonant scattering is limited to regions of relatively low densities: above some critical density line emission will start to dominate scattering, erasing any decrement of the CMB brightness temperature produced by scattering protoclouds (Basu 2007). For example, densities of about 0.1-1 cm^{-3} are sufficient to erase the scattering signature produced by the lowest rotational transitions of HD and HD^+.

The intensity and angular size of emission/absorption lines produced by various molecules during the evolution of primordial density perturbations with masses ranging from 10^9 to 10^{12} $M_\odot$ were computed by Maoli, Melchiorri & Tosti (1994), Maoli et al. (1996). They found that the very initial phases of nonlinear collapse provide the best conditions for the detection of resonant scattering. In fact, at the moment when the cloud collapse is exactly compensated by the cosmological expansion (turnaround), the line width reaches the minimum (i.e. thermal) value, and the absorption cross section is the highest (Zel'dovich 1978). The signal

thus changes from a relatively low-intensity broad line in the linear phase to an intermediate-intensity line of growing broadening during nonlinear collapse, passing through a high-intensity thin peak at turnaround.

These studies prompted a few attempts to detect spectral signatures of primordial molecules. The first one, performed at mm wavelengths with the IRAM radiotelescope, consisted in a search for redshifted rovibrational transitions of LiH emitted by protogalaxies at $z \approx 100$–200 (de Bernardis et al. 1993). These observations gave upper limits of ~ 20 mK on the intensity of LiH lines, only slightly above the expected intensity of LiH for optical depths of order unity, a value that was later found largely overestimated. Using a chemical network based on the reaction rates for Li chemistry known at the time, Palla, Galli & Silk (1995) found LiH abundances of the order of 10^{-14}–10^{-13} and a value of only $\sim 10^{-5}$ for the optical depth of LiH at mm wavelengths. Bellini et al. (1994) suggested to extend the search at cm wavelengths, where the optical depth of redshifted pure rotational transitions of the $v = 0$ level would be about two orders of magnitude larger. However, no results were obtained by Gosachinskij et al. (2002) in their search for spectral signatures of LiH at a wavelength of 6.2 cm using the RATAN-600 radio telescope. Using more reliable abundances, the optical depth of LiH was found to be of the order of only $\sim 10^{-11}$ and $\sim 10^{-13}$ at cm and mm wavelengths, respectively (Bougleux & Galli 1997). The search for HD lines appears more promising, as the optical depths of the three lowest pure rotational lines are much higher than for LiH, although their intensities are still below the sensitivities of current facilities like GMT/LMT, CARMA and ALMA (Núñez-López, Lipovka & Avila-Reese 2006). Recently, Persson et al. (2010) have reported the results of broad band, blind line surveys with the *Odin* satellite to search for the lowest rotational transitions of H_2, as well as higher transitions of HD and HeH^+ redshifted from $z \approx 20$–30, the epoch of the first structure formation. Although no lines were detected, the search set some interesting limits on the amplitudes of the possible resonant lines and can serve as a pilot study for current and future radiotelescopes.

6.3 Spatial Anisotropies

In addition to spectral features, resonant scattering from primordial molecules can also produce secondary spatial anisotropies in the CMB, leading to changes in the expansion coefficients C_l of the CMB power spectrum

$$\frac{\Delta C_l}{C_l} \approx -2\tau_\nu, \tag{44}$$

for $\tau_\nu \ll 1$ and $l \gg 1$ (Maoli, Melchiorri & Tosti 1994; Basu, Hernández-Monteagudo & Sunyaev 2004; Basu 2007). Thus, a promising way to detect secondary anisotropies due to resonant scattering is to compare the expansion coefficients of the angular power spectrum C_l at different wavelengths to detect signals of ~ 0.1 μK or less, exploiting the sensitivity of satellites like *Planck*, and other ground-based or balloon-borne instruments like the Atacama Cosmological Telescope (ACT), Atacama Pathfinder Experiment Telescope (APEX) and the South Pole Telescope (SPT). However, since the angular scales of the expected anisotropies are small, of the order of a few arcmin at best (Maoli et al. 1996), only multipole coefficients with $l \gtrsim 1000$ will be affected, making the detection difficult. A possible experimental setup for the Multi-Beam Solar Radio Telescope

(MSRT, Tuorla, Finland) is described in Dubrovich, Bajkova & Khaikin (2008).

6.4 Emission by Molecular Formation

In analogy with H and He recombination, molecule formation also occurs in excited states that then decay to the fundamental level emitting photons that produce an excess over the pure Planck distribution of the CMB. For example, H_2 is formed by associative detachment in vibrationally excited states that quickly decay to the ground state (see, Section 4.2). Since the maximum production of H_2 occurs at redshifts $z \lesssim 100$, the emission of rovibrational transitions with $\lambda \approx 2$ μm is redshifted today at $\lambda \lesssim 200$ μm in the Wien part of the CMB. Coincidentally, this is the same wavelength range where photons produced by Ly-α and two-photon decay of H and He during recombination are also redshifted (Section 3.3). The H_2 emission has been computed by Coppola et al. (2012, see also Khersonskii 1982 and Shchekinov & Entel 1984) for multiquantum transitions up to $\Delta v = 4$. As in the case of H and He recombination photons, a direct detection of the H_2 formation emission in this wavelength range appears challenging, owing to the presence of an infrared background (both Galactic and extragalactic) several orders of magnitude brighter than the CMB (see e.g. discussion in Wong, Seager & Scott 2006). However, the excess photons produced by H_2 formation could significantly affect a number of photodestruction rates at high redshift.

6.5 Absorption by Thermal Nonequilibrium

At redshift below $z \approx 500$ matter and radiation are no longer efficiently coupled by Compton scattering, and the temperatures of baryon and photons decrease approximately according to the adiabatic laws $T_\mathrm{r} \propto (1+z)^{-1}$ and $T_\mathrm{g} \propto (1+z)^{-2}$, respectively (see Section 3.3). In these circumstances, molecules act as heat pumps, transferring energy from the hotter radiation to the colder gas (Khersonskii 1986; Puy et al. 1993). The effect on the CMB temperature is of the order of

$$\frac{\Delta T_\mathrm{r}}{T_\mathrm{r}} \approx -\left(1 - \frac{T_\mathrm{ex}}{T_\mathrm{r}}\right)\tau_\nu, \tag{45}$$

where T_ex is the excitation temperature of the transition, defined by the condition $g_\mathrm{l} n_\mathrm{u}/g_\mathrm{u} n_\mathrm{l} = \exp(-h\nu_\mathrm{ul}/kT_\mathrm{ex})$. In a collapsing cloud, when the density becomes larger than a critical density for thermal equilibrium with collisions, T_ex becomes equal to T_g, and the latter rapidly increases above T_r. In this case line emission start to dominate (e.g., Mizusawa et al. 2005, Basu 2007). On the other hand, in the expanding primordial gas after recombination, when radiative effects still largely dominate over collisional excitation/de-excitation, the excitation temperature of a molecular transition is very close to the temperature of the CMB, $T_\mathrm{g} < T_\mathrm{ex} \lesssim T_\mathrm{r}$. This explains the limited absorbing power of a layer of primordial molecules and the major obstacle for their detection: those species with high dipole moments, and thus high absorption cross sections, have $T_\mathrm{ex} \approx T_\mathrm{r}$, while species with low dipole moments have $\tau_\nu \ll 1$. Puy et al. (1993) considered only pure rotational transitions in the $v = 0$ level of H_2, HD and LiH and found negligible effects of molecular absorption on the CMB: $\Delta T_\mathrm{r}/T_\mathrm{r} \lesssim 10^{-9}$ at $\nu \sim 40$–80 GHz for rotational transitions of H_2 and even less for rotational transitions of HD and LiH. Also in the case of H^-, the relative change in the CMB temperature due to the bound-free and free-free processes discussed above is small, because the

absorption and the emission processes are close to equilibrium, making the net effect of the order of only $\sim 10^{-10}$ over a frequency range from 100 to 1000 GHz (Schleicher et al. 2008). As already mentioned in Section 6.1, the 21 cm hyperfine transition of neutral hydrogen represents an exception to this behavior. Because of its extremely small Einstein coefficient ($A_{10} = 2.85 \times 10^{-15}$ s^{-1}), collisions are able to couple $T_{\rm ex}$ (called in this case "spin temperature") to $T_{\rm g}$ down to $z \approx 100$, when the Hubble time becomes longer than the lifetime of the $F = 1$ level and $T_{\rm ex}$ approaches $T_{\rm r}$ until reionization occurs (Purcell & Field 1956; Pritchard & Loeb 2008).

7 SUMMARY POINTS

- Assuming that cosmology and standard Big Bang nucleosynthesis have entered the precision era, the dawn of chemistry can now be accurately followed from the recombination epoch to the end of the dark ages. Chemical networks containing more than ~ 250 reactions for ~ 30 species have been developed to make quantitative predictions on their abundances. Most of the remaining uncertainty can be attributed to the partial knowledge of cross sections and rate coefficients at the relevant energies and temperatures.
- Due to the lack of dust grains, primordial chemistry is driven by slow gas-phase reactions promoted by collisions with electrons and protons left over from recombination at a level of one part in $\sim 10^4$. As a result, only simple diatomic and triatomic molecules and molecular ions containing H, D, He, and Li are formed in trace amounts.
- The low density of the expanding medium and the harsh radiation field due to the cosmic background limit the maximum production of each species. While H_2 and HD reach freeze-out abundances of $\lesssim 10^{-6}$ and $\gtrsim 10^{-10}$, respectively, at $z \approx 40$, all other molecules/ions have abundances much smaller than 10^{-10}.
- The evolution of H_2, H_2^+, H_3^+ and their deuterated isotopologues depends to a large extent on the additional contribution to the cosmic radiation field of photons produced by the recombination of H and He. These photons also reduce the abundance of H^- and Li: the former limits the freeze-out fraction of H_2, the latter never recombines.
- Primordial molecules allow the gas to cool, contract, and fragment. While the answer to fundamental questions regarding the formation of the first structures and stars (fragmentation scale, mass spectrum, maximum mass, etc.) does not depend on chemistry alone, a full understanding of the thermodynamical properties of the baryonic matter is a fundamental ingredient in all numerical simulations addressing these issues. It is rewarding that detailed chemical networks and accurate cooling functions are now integral parts of state-of-the-art simulations.
- The interaction of the CMB with the primordial gas is probably the best probe to test the predictions of primordial chemistry and provides a unique way to peer into the dark ages prior to structure formation. The effects of absorption, emission and resonant scattering on the temperature and power spectrum of the CMB have been fully explored theoretically.

- The most promising results are obtained for the negative hydrogen ion H^- and the HeH^+ molecular ion. The free-free process of H^- leads to a frequency-dependent change in the power spectrum of the CMB of the order of 10^{-7} at 30 GHz. HeH^+ can efficiently scatter CMB photons and smear out primordial fluctuations in the frequency range 30–300 GHz, leading to a change in the power spectrum of the order of 10^{-8}. Finally, resonant scatter by neutral Li dominates the optical depth of the universe in the far-infrared.

8 FUTURE ISSUES

- Major progress has been achieved by the inclusion of state-resolved chemical reaction rates for H_2 and H_2^+, that are formed out of equilibrium in highly-excited vibrational levels and then decay radiatively to the fundamental state. It is desirable to extend this approach to other species like HD, HD^+ and HeH^+. Further improvement comes from recent fully-quantal ab initio calculations of reaction cross sections for He and Li chemistry specifically performed for applications to the early universe. Extending these calculations to other species/processes is an obvious need. It is necessary to complement these theoretical studies with laboratory experiments, especially at sub-eV energies.
- While excellent agreement between theory and experiments has been reached for some key reactions, most notably the dissociative attachment of H^- leading to H_2 formation and the dissociative recombination of H_3^+, a number of other important reactions still suffer from either poor knowledge or inconsistencies. For example, in the high density phase of collapse within dark matter minihalos, the conversion to fully molecular gas by three-body reactions is still affected by significant uncertainties. We have provided an assessment for this and several other critical reactions.
- Searches for signals from primordial molecules and for their imprint on the CMB are very challenging, in part owing to the extreme weakness of the expected lines and also because of the poorly constrained redshift of emission. However, the exploration of the dark ages using molecular and atomic transitions is already under way with the largest available facilities like ALMA and LOFAR, and dedicated satellites like *Planck*. We can hope that with the advent of next-generation telescopes (e.g., JWST, SKA, ELTs, etc.) some fundamental breakthrough can be achieved that will shed light on the dawn of chemistry and its impact on the birth of the first structures.

9 ACKNOWLEDGMENTS

It is a pleasure to thank Stefano Bovino, Carla Maria Coppola, Fabrizio Esposito, Franco A. Gianturco, Savino Longo, Dominik Schleicher who have contributed so much over the years to a fruitful and enjoyable collaboration. We also acknowledge exciting conversations on primordial chemistry and star formation with John Black, Simon Glover, Takashi Hosokawa, Ralf Klessen, Kazuyuki Omukai, Daniel Savin, and Raffaella Schneider. We thank Fabio Iocco and Ofelia Pisanti for computing BBN abundances. Finally, we are grateful to Ewine van Dishoeck, Amiel

Sternberg and Malcolm Walmsley for critically reading an earlier version of this manuscript and providing comments that improved it.

Literature Cited

Abel T, Anninos P, Zhang Y, Norman, ML. 1997. *New Astron.* 2:181
Abel T, Bryan GL, Norman, ML. 2002. *Science* 295:93
Ali-Haïmoud Y, Hirata CM. 2010. *Phys. Rev. D* 82:063521
Ali-Haïmoud Y, Hirata CM. 2011. *Phys. Rev. D* 83:043513
Alizadeh E, Hirata C. 2011. *Phys. Rev. D* 84:083011
Asplund M, Lambert DL, Nissen P, Primas F, Smith VV. 2006. *Ap. J.* 644:229
Aver E, Olive KA, Skillman ED. 2010. *J. Cosmol. Astrop. Phys.* 5:3
Aver E, Olive KA, Skillman ED. 2012. *J. Cosmol. Astrop. Phys.* 4:4
Ayouz M, Lopes R, Raoult M, Dulieu O, Kokoouline, V. 2011. *Phys. Rev. Lett.* 83:052712
Bacchus-Montabonel MC, Talbi, D. 1999. *J. Molec. Struc.* 463:91
Balakrishnan N, Quéméner G, Forrey RC, Hinde RJ, Stancil PC. 2011. *J. Chem. Phys.* 134:014301
Bania TM, Rood RT, Balser DS. 2010. In *Light Elements in the Universe*, eds. C Charbonnel et. al., IAU Symp. 268, p. 81
Basu D, Barua AK. 1984. *J. Phys. B* 17:1537
Basu K, Hernández-Monteagudo C, Sunyaev RA. 2004. *Astron. Astrophys.* 416:447
Basu K. 2007. *New Astr. Rev.* 51:431
Bates DR. 1951. *MNRAS* 111:303
Bellini M, de Natale P, Inguscio M, Fink E, Galli D, Palla F. 1994. *Ap. J.* 424:507
Bennett OJ, Dickinson AS, Leininger T, Gadéa FX. 2003. *MNRAS* 341:361 (Erratum in 2008. *MNRAS* 384:1743)
Black, JH. 1990. In *Molecular Astrophysics*, ed. TW Hartquist (Cambridge: University Press), p.473
Black, JH. 2006. *Faraday Discuss.* 133:27
Bodo E, Gianturco FA, Martinazzo, R. 2003. *Phys. Rep.* 384:85
Bonifacio P, Sbordone L, Caffau E, Ludvig HG, Spite M, et al. 2012. *Astron. Astrophys.* 542:A87
Bougleux E, Galli D. 1997. *MNRAS* 288:638
Bovino S, Wernli M, Gianturco, FA. 2009. *Ap. J.* 699:383
Bovino S, Stoecklin T, Gianturco FA. 2010a. *Ap. J.* 708:1560 (Erratum in 2010. *Ap. J.* 713:711)
Bovino S, Tacconi M, Gianturco FA, Stoecklin T. 2010. *Ap. J.* 724:126
Bovino S, Tacconi M, Gianturco FA. 2011a. *Ap. J.* 740:101 (Erratum in 2012. *Ap. J.* 748:150)
Bovino S, Tacconi M, Gianturco FA. 2011b. *Phys. Scr.* 84:028103
Bovino S, Tacconi M, Gianturco FA, Galli D. 2011c. *Astron. Astrophys.* 529:A140
Bovino S, Tacconi M, Gianturco FA, Galli D, Palla F. 2011d. *Ap. J.* 731:107
Bovino S, Čurík R, Galli D, Tacconi M, Gianturco FA. 2012. *Ap. J.* 752:19
Bromm V. 2012. *arXiv1203.3824*
Bromm V, Loeb A. 2003. *Nature* 425:812
Bromm V, Loeb A. 2003. *Ap. J.* 596:34
Bromm V, Yoshida N. 2011. *Annu. Rev.Astron. Astrophys.* 49:373
Bromm V, Coppi PS, Larson RB. 2002. *Ap. J.* 564:23

Bromm V, Yoshida N, Hernquist L, McKee CF. 2009. *Nature* 459:49
Bruhns H, Kreckel H, Miller KA, Urbain X, Savin DW. 2010. *Phys. Rev. A* 82:042708-1
Caffau E, Bonifacio P, François P, Spite M., Spite F., et al. 2011. *Nature* 477:67
Caffau E, Bonifacio P, François P, Spite M., Spite F., et al. 2012. *Astron. Astrophys.* 542:A51
Carlberg RG. 1981. *MNRAS* 197:1021
Cassisi S, Castellani V. 1993. *Ap. J.*S 88:509
Chandrasekhar S. 1958. *Ap. J.* 128:114
Charutz DM, Last I, Baer M. 1997. *J. Chem. Phys.* 106:7654
Chluba J, Thomas RM. 2011. *MNRAS* 412:748
Chluba J, Vasil GM, Dursi LJ. 2010. *MNRAS* 407:599
Chluba J, Fung J, Switzer ER. 2012. *MNRAS* 423:3227
Christlieb N, Bessell MS, Beers TC., Gustafsson B, Korn A, et al. 2002. *Nature* 419:904
Cízek M, Horácek J, Domcke W. 1998. *J. Phys. B* 31:2571
Clark PC, Glover SCO, Klessen RS. 2008. *Ap. J.* 672:757
Clark PC, Glover SCO, Klessen RS, Bromm V. 2011. *Ap. J.* 727:110
Clark PC, Glover SCO, Smith RJ. 2011. *Science* 331:1040
Coc A, Goriely S, Xu Y, Saimpert M, Vangioni E. 2012. *Ap. J.* 744:158
Combes F, Wiklind T. 1998. *Astron. Astrophys.* 334:L81
Cooke R, Pettini M, Steidel CC. 2011. *MNRAS* 417:1534
Coppola CM, Lodi L, Tennyson J. 2011. *MNRAS* 415:487
Coppola CM, Longo S, Capitelli M, Palla F, Galli D. 2011. *Ap. J. Suppl.* 193:7
Coppola CM, D'Introno R, Galli D, Tennyson J, Longo S. 2012. *Ap. J.*S 199:16
Couchman HMP, Rees MJ. 1986. *MNRAS* 221:53
Čurík R, Greene CH. 2007. *Phys. Rev. Lett.* 98:173201
Čurík R, Greene CH. 2008. *J. of Phys. Conf. Ser.* 115:012016
de Bernardis P, Dubrovich VK, Encrenaz P, Maoli R, Masi S, et al. 1993. *Astron. Astrophys.* 269:1
Dalgarno A, Lepp S. 1987. In *Astrochemistry*, eds. MS Vardya & SP Tarafdar (Dordrecht: Reidel), p. 109
Dalgarno A, Kirby K, Stancil PC. 1996. *Ap. J.* 458:397
Dalgarno A, van der Loo MPJ. 2006. *Ap. J.* 646:L91
Dalgarno A, Weisheit JC, Black JH. 1973. *Astrophys. Lett.* 14:77
Datz S, Larsson M, Stromholm C, Sundström G, Zengin V, et al. 1995. *Phys. Rev. A* 52:2901
Diep P, Johnson JK. 2000. *J. Chem. Phys.* 112:4465
Dinerstein HL, Geballe TR. 2001. *Ap. J.* 562:515
Dubrovich VK. 1977. *Sov. Astr. Lett.*. 3:181 (orig. 1977. *Pis'ma Astron. Zh.* 3:339)
Dubrovich VK. 1993. *Sov. Astr. Lett.*. 19:53 (orig. 1993. *Pis'ma Astron. Zh.* 19:132)
Dubrovich VK. 1994. *Astron. Astrophys.* Trans. 5:57
Dubrovich VK. 1997. *Astron. Astrophys.* 324:27
Dubrovich VK, Lipovka AA. 1995. *Astron. Astrophys.* 296:301
Dubrovich V, Bajkova A, Khaikin VB. 2008. *New Astron.* 13:28
Dumitriu I, Saenz A. 2009. J. Phys. Conf. Ser. 194:152026
Dunn GH. 1968. *Phys. Rev.* 172:1
Ekström S, Coc A, Descouvemont P, Meynet G., Olive KA, et al. 2010. *Astron. Astrophys.* 514:A62

Esposito F, Capitelli M. 2009. *J. Chem. Phys.* A 113:15307
Fehsenfeld FC, Howard CJ, Ferguson EE. 1973. *J. Chem. Phys.* 58:5841
Fendt WA, Chluba J, Rubiño-Martín JA, Wandelt BD. 2009. *Ap. J.*S 181:627
Field GB. 1959. *Ap. J.* 129:563
Fields BD. 2011. *Ann. Rev. of Nucl. Part. Sci.* 61:47
Fixsen DJ. 2009. *Ap. J.* 707:916
Flower DR, Roueff E. 1979. *Astron. Astrophys.* 72:361
Flower DR, Harris GJ. 2007. *MNRAS* 377:705
Frebel A, Johnson JL, Bromm V. 2007. *MNRAS* 380:L40
Frebel A, Collet R, Eriksson K, Christlieb N, Aoki W. 2008. *Ap. J.* 684:588
Friedel DN, Kemball A, Fields BD. 2011. *Ap. J.* 738:37
Fumagalli M, O'Meara JM, Prochaska JX. 2011. *Science* 334:1245
Galli D, Palla F. 1989. In *Astronomy, Cosmology and Fundamental Physics*, eds. M Caffo et al. (Dordrecht: Kluwer), p. 421
Galli D, Palla F. 1998. *Astron. Astrophys.* 335:403
Galli D, Palla F. 2000. In *The First Stars*, eds. A Weiss et al. (Berlin: Springer), p. 229
Galli D, Palla F. 2002. *Planet. Sp. Sci.* 50:1197
García Pérez AE, Aoki W., Inoue S, Ryan SG, Suzuki TK, Chiba M. 2009. *Astron. Astrophys.* 504:213
Gay CD, Stancil PC, Lepp S, Dalgarno A. 2011. *Ap. J.* 737:44
Gerlich D, 1982. In *Symposium on Atomic & Surface Physics*, eds. W Lindinger et al. (Dordrecht: Kluwer), p. 304
Gerlich D, Horning S. 1992. *Chem. Rev.* 92:1509
Gerlich D, Jusko P, Roučka, Š, Zymak I, Plašil R, Glosík J. 2012. *Ap. J.* 749:22
Gianturco FA, Gori Giorgi P, Berriche H, Gadea FX. 1996. *Astron. Astrophys.*S 117:377
Gianturco FA, Gori Giorgi P. 1996. *Phys. Rev. A* 54:1
Gianturco FA, Gori Giorgi P. 1997. *Ap. J.* 479:560
Glassgold AE, Galli D, Padovani M. 2012. *Ap. J.* 756:157
Glosík J, Korolov I, Plašil R, Novotny O, Kotrik T, et al. 2008. *J. Phys. B.* 41:191001
Glover SCO, Abel T. 2008. *MNRAS* 388:1627
Glover SCO, Savin DW. 2009. *MNRAS* 393:911
Glover SCO, Savin DW, Jappsen AK. 2006. *Ap. J.* 640:553
Gosachinskij IV, Dubrovich VK, Zhelenkov SR, Il'in GN, Prozorov VA. 2002. *Astr. Rep.* 46:543
Grin D, Hirata CM. 2010. *Phys. Rev. D* 81:083005
Guberman SL. 1994. *Phys. Rev. A* 49:4277
Holliday MG, Muckerman JT, Friedman L. 1971. *J. Chem. Phys.* 54:1058
Hirasawa T, Aizu K, Taketani M. 1969. *Prog. Theor. Phys.* 41:835
Hirata CM, Padmanabhan N. 2006. *MNRAS* 372:1175
Hirata CM, Switzer ER. 2008. *Phys. Rev. D* 77:083007
Hosokawa T, Omukai K, Yoshida N, Yorke HW. 2011. *Science* 334:1250
Hosokawa T, Omukai K, Yorke HW. 2012. *Ap. J.* 756:93
Howk JC, Lehenr N, Fields BD, Mathews GJ. 2012. *Nature* 489:121
Hutchins JB. 1976. *Ap. J.* 191:375
Iocco F, Mangano G, Miele G, Pisanti O, Serpico PD. 2009. *Phys. Rep.* 472:1
Izotov Y, Thuan TX. 2010. *Ap. J.* 710:L67
Izotov Y, Thuan TX, Stasinska G. 2007. *Ap. J.* 662:15

Janev RK, Langer WD, Evans K. 1987. *Springer Series on Atoms and Plasmas* (Berlin: Springer)
Jester S, Falcke H. 2009. *New Astron.* 53:1
Johnson JL, Bromm V. 2006, *MNRAS* 366:247
Jones BJT, Wise RFG. 1985. *Astron. Astrophys.* 149:144
Juřek M, Špirko V, Kraemer WP. 1995. *Chem. Phys.* 193:287
Karpas Z, Anicich V, Huntress WT. 1979. *J. Chem. Phys.* 70:2877
Keisler R, Reichardt CL, Aird KA. 2011. *Ap. J.*, 743:28
Khersonskii VK. 1982. *Ap. Space Sci.* 88:21
Khersonskii VK. 1986. *Astrophys.* 24:114 (orig. 1986. *Astrofizika* 24:191)
Khersonskii VK, Lipovka AA. 1993. *Bull. Spec. Astrophys. Observ.* 36:88
Kholupenko EE, Ivanchik AV, Balashev SA, Varshalovich DA. 2011. *MNRAS* 417:2417
Kimura M, Lane NF, Dalgarno A, Dixson RG. 1993. *Ap. J.* 405:801
Kirkman D, Tytler D, Suzuki N, O'Meara JM, Lubin D. 2003. *Ap. J. Suppl.* 149:1
Klessen R, Glover SCO, Clark PC. 2012. *MNRAS* 421:3217
Komatsu E, Smith KM, Dunkley J, Bennett CL, Gold B, et al. 2011. *Ap. J. Suppl.* 192:18
Kreckel H, Motsch M, Mikosch J., Glosík J, Plašil R, et al. 2005. *Phys. Rev. Lett.* 95:3201
Kreckel H, Bruhns H, Cízek M., Glover SCO, Miller KA, et al. 2010. *Science* 329:69
Krolik JH. 1990. *Ap. J.* 353:21
Krstić PS. 2002. *Phys. Rev. A* 66:042717
Larsson M, Lepp S, Dalgarno A, Strömholm C, Sundström G, et al. 1996. *Astron. Astrophys.* 309:L1
Latter WB. 1989. *PhD Thesis*, Univ. of Arizona
Latter WB, Black JH. 1991. *Ap. J.* 372:161
Lebedev VS, Presnyakov LP, Sobel'Man II. 2000. *Astr. Rep.* 44:338
Lee TG, Balakrishnan N, Forrey RC, Stancil PC, Shaw G., et al. 2008. *Ap. J.* 689:1105
Lepp S, Shull JM. 1984. *Ap. J.* 270:578
Lepp S, Stancil PC, Dalgarno A. 2002. *J. Phys. B* 35:57
Linder F, Janev RK, Botero J. 1995. *Atomic and Molecular Processes in Fusion Edge Plasmas*, ed. RK Janev (New York: Plenum Press), p. 397
Lipovka A, Núñez-López R, Avila-Reese V. 2005. *MNRAS* 361:850
Liu XW, Barlow MJ, Dalgarno A, Tennyson J., Lim T., et al. 1997. *MNRAS* 290:L71
Loeb A. 2001. *Ap. J.* 555:L1
Loeb A. 2010. *How did the First Stars and Galaxies Form?* (Princeton: Princeton Univ. Press)
Longo S, Coppola CM, Galli D, Palla F, Capitelli M. 2011. *Rend. Fis. Acc. Lincei* 22:1
Maoli R, Melchiorri F, Tosti D. 1994. *Ap. J.* 425:372
Maoli R, Ferrucci V, Melchiorri F, Signore M, Tosti D. 1996. *Ap. J.* 457:1
Martinez O, Yang Z, Betts NB, Snow TP, Bierbaum VM. 2009. *Ap. J.* 705:L172
Matsuda T, Sato H, Takeda H. 1969. *Prog. Theor. Phys.* 42:219
Matsuda T, Sato H, Takeda H. 1971. *Prog. Theor. Phys.* 46:416
McCall BJ, Huneycutt AJ, Saykally RJ, Djuric N, Dunn GH, et al. 2004. *Phys. Rev. A* 70:052716

McCrea WH. 1960. Proc. Roy. Soc. A 256:245
McCrea WH, McNally D. 1960. *MNRAS* 121:238
McDowell MRC. 1961. *Observatory* 81:240
McGreer ID, Bryan GL. 2008. *Ap. J.* 685:8
McKee CF, Tan JC. 2008. *Ap. J.* 681:771
Michael JV, Fisher JR. 1990. *J. Phys. Chem.* 93:3318
Mielke SL, Lynch GC, Truhlar DG, Schwenke DW. 1994. *J. Phys. Chem.* 98:8000
Miller KA, Bruhns H, Eliáišek J, Čížek M, Kreckel H, et al. 2011. *Phys. Rev. A* 84:e2709
Miller S, Stallard T, Melin H, Tennyson J. 2010. *Faraday Discuss.* 147:283
Mizusawa H, Omukai K, Nishi R. 2005. *Publ. Astron. Soc. Japan* 57:951
Mitchell DN, LeRoy DJ. 1973. *J. Chem. Phys.* 58:3449
Miyake S, Stancil PC. 2007. *Bull. AAS* 39:139.09
Miyake S, Gay CD, Stancil PC. 2011. *Ap. J.* 735:21
Moorhead JM, Lowe RP, Wehlau WH, Maillard JP, Bernath PF. 1988. *Ap. J.* 326:899
Moseley J, Aberth W, Peterson JR. 1970. *Phys. Rev. Lett.* 24:435
Nagakura T, Omukai K. 2005. *MNRAS* 364:1378
Nakamura F, Umemura N. 2002. *Ap. J.* 569:549
Nolte JL, Stancil PC, Lee TG, Balakrishnan N, Forrey RC. 2012. *Ap. J.* 744:62
Norris JE, Christlieb N, Korn AJ, Eriksson K, Bessell MS. 2007. *Ap. J.* 670:774
Noterdaeme P, López S, Dumont V, Ledoux C, Molaro P, Petitjean P. 2012. *Astron. Astrophys.* 542:L33
Novikov I, Zel'dovich YB. 1967. *Annu. Rev.Astron. Astrophys.* 5:627
Núñez-López R, Lipovka A, Avila-Reese V. 2006. *MNRAS* 369:2005
Oh SP, Haiman Z. 2002. *Ap. J.* 569:558
Olive K, Skillman ED. 2004. *Ap. J.* 617:29
Olive KA, Petitjean P, Vangioni E, Silk J. 2012. *MNRAS*, 426:1427
Orel AE. 1987. *J. Chem. Phys.* 87:314
Pagel BEJ. 1959. *MNRAS* 119:609
Palla F, Salpeter EE, Stahler SW. 1983. *Ap. J.* 271:632
Palla F, Galli D, Silk J. 1995. *Ap. J.* 451:44
Palla F, Galli D. 2000. In H_2 *in Space*, eds. F Combes & G Pineau Des Fôrets (Cambridge: Cambridge Univ. Press), p. 119
Pavanello M, Bubin S, Molski M, Adamowicz L. 2005. *J. Chem. Phys.* 123:104306
Peart B, Hayton DA. 1992. *J. Phys. B* 25:5109
Pedersen HB, Altevogt S, Jordon-Thaden B, Heber O, Lammich L., et al. 2007. *Phys. Rev. Lett.* 98:223202
Peebles PJE. 1968. *Ap. J.* 153:1
Peebles PJE. 1993. *Principles of Physical Cosmology* (Princeton: Princeton Univ. Press), Chap. 6
Peebles PJE, Dicke RH. 1968. *Ap. J.* 154:891
Persson CM, Maoli R, Encrenaz P, Hjalmarson Å, Olberg M, et al. 2010. *Astron. Astrophys.* 515:A72
Pettini M, Zych BJ, Murphy MT, Lewis A, Steidel CC. 2008. *MNRAS* 391:1499
Pettini M, Cooke R. 2012 *MNRAS* 425:2477
Pritchard JR, Loeb A. 2008. *Phys. Rev. Lett.* 78:103511
Pritchard JR, Loeb A. 2012. *Rep. Progr. Phys.* 75:086901
Purcell EM, Field GB. 1956. *Ap. J.* 124:542
Puy D, Alecian G, Le Bourlot J, Leorat J, Pineau Des Forêts G. 1993. *Astron.*

Astrophys. 267:337
Puy D, Signore M. 2002. *New Astron.* Rev. 46:709
Puy D. Signore M. 2007. *New Astron.* 51:411
Puy D, Dubrovich V, Lipovka A, Talbi D, Vonlanthen P. 2007. *Astron. Astrophys.* 476:685
Rafelsky M, Wolfe AM, Prochaska JX, Neeleman M, Mendez AJ. 2012. *Ap. J.* 755:89
Ramaker DE, Peek JM. 1979. *J. Chem. Phys.* 71:1844
Ripamonti E, Mapelli M, Ferrara A. 2007. *MNRAS* 375:1399
Roberge W, Dalgarno A. 1982. *Ap. J.* 255:489
Rubiño-Martín JA, Chluba J, Fendt WA, Wandelt BD. 2010. *MNRAS* 403:439
Rutherford JA, Vroom DA. 1973. *J. Chem. Phys.* 58:4076
Saha S, Datta KK, Barua AK. 1978. *J. Phys. B* 11:3349
Sakimoto K. 1989. *Chem. Phys. Lett.* 164:294
Saslaw WC, Zipoy D. 1967. *Nature*, 216:976
Sasaki S, Takahara F. 1993. *Publ. Astron. Soc. Japan* 45:655
Savin DW. 2002. *Ap. J.* 566:599
Savin DW, Brickhouse NS, Cowan JJ, Drake RP, Federman SR, et al. 2012. *Rep. Progr. Phys.* 75:036901
Savin DW. 2013. In *First Stars IV*, eds. M Umemura & K Omukai, AIP 1840, in press
Savin DW, Krstić PS, Haiman Z, Stancil PC. 2004. *Ap. J.* 606:L167 (Erratum 2004. *Ap. J.* 607:L147)
Sbordone L, Bonifacio P, Caffau E, Ludvig HG, Behara NT, et al. 2010. *Astron. Astrophys.* 522:A26
Schleicher DRG, Galli D, Palla F, Camenzind M, Klessen RS, et al. 2008. *Astron. Astrophys.* 490:521
Schleicher DRG, Galli D, Glover SCO, Banerjee R, Palla F, et al. 2009. *Ap. J.* 703:1096
Schmeltekopf AL, Fehsenfeld FF, Ferguson EE. 1967. *Ap. J.* 148:L155
Schneider IF, Dulieu O, Giusti-Suzor A, Roueff E. 1994. *Ap. J.* 424:983 (Erratum 1997. *Ap. J.* 486:580)
Schneider IF, Suzor-Weiner A. 2002. *Contr. to Plasma Physics* 42:578
Schneider R, Omukai K, Limongi M, Ferrara A, Salvaterra R, Chieffi A., Bianchi S. 2012. *MNRAS* 423:L60
Scott D, Moss A. 2009. *MNRAS* 397:445
Seager S, Sasselov SS, Scott D. 1999. *Ap. J.* 523:L1
Seager S, Sasselov SS, Scott D. 2000. *Ap. J.* 128:407
Serpico PD, Esposito S, Iocco F. 2004. *J. Cosmol. Astropart. Phys.* 12:10
Shapiro PR, Kang H. 1987. *Ap. J.* 318:32
Shavitt I. 1959. *J. Chem. Phys.* 31:1359
Shchekinov YA, Entel MB. 1984. *Sov. Astr.* 28:270 (orig. 1984. *Astron. Zh.* 61:460)
Silk J. 1977. *Ap. J.* 214:718
Smith D, Španel P. 1993. *Int. J. Mass Spectr. Ion. Proc.* 129:163
Smoot GF, Bennett CL, Kogut A., Wright EL, Aymont J, et al. 1992. *Ap. J.*, 396:L1
Sodoga K, Loreau J, Lauvergnat D, Justum Y, Vaeck N, et al. 2009. *Phys. Rev. A* 80:033417
Spergel DN, Verde L, Peiris HV, Komatsu E, Nolta MR, et al. 2003. *Ap. J. Suppl.*

148:175
Stacy A, Greif T, Bromm V. 2010. *MNRAS* 403:45
Stancil PC, Babb JF, Dalgarno A. 1993. *Ap. J.* 414:672
Stancil PC, Lepp S, Dalgarno A. 1996, *Ap. J.* 458:401
Stancil PC, Lepp S, Dalgarno A. 1998. *Ap. J.* 509:1
Stancil PC, Loeb A, Zaldarriaga M, Dalgarno A, Lepp S. 2002. *Ap. J.* 580:29
Stärck J, Meyer W. 1993. *Chem. Phys.* 176:83
Steigman G. 2007. *Annu. Rev. Nucl. Part. Sci.* 57:463
Stenrup M, Larson A, Elander N. 2009. *Phys. Rev. A* 79:012713
Sundström G, Mowat JR, Danared H. 1994. *Science* 263:785
Sunyaev RA, Zel'dovich YB. 1970. *Ap. Space Sci.* 7:3
Switzer ER, Hirata CM. 2005. *Phys. Rev. D* 72:083002.1
Switzer ER, Hirata CM. 2008a. *Phys. Rev. D* 77:083006
Switzer ER, Hirata CM. 2008b. *Phys. Rev. D* 77:083008
Szucs S, Karemera M, Terao M, Brouillard F. 1984. *J. Phys. B* 17:1613
Takagi T. 2002. *Phys. Scr.*, 96:52
Takayanagi N, Nishimura S. 1960. *Publ. Astron. Soc. Japan* 12:77
Takeda H, Sato H, Matsuda T. 1969. *Progr. Theor. Phys.* 41:840
Talbi D, Bacchus-Montabonel MC. 1998. *Chem. Phys.* 232 267
Tegmark M, Silk J, Rees MJ, Blanchard A, Abel T, Palla F. 1997. *Ap. J.* 474:1
Turk MJ, Abel T, O'Shea B. 2009. *Science* 325:601
Turk MJ, Clark PC, Glover SCO, Greif TH, Abel T, Klessen R, Bromm V. 2011. *Ap. J.* 726:55
Turk MJ, Oishi JS, Abel T, Bryan GL. 2012. *Ap. J.* 745:154
Umemura M, Omukai K. 2013. *First Stars IV*, AIP Conf. Proc. 1480
Urbain X. 2010. *APS Div. At. Mol. Opt. Phys. Meeting Abstracts*, p. 1003
Varshalovich DA, Khersonskii VK. 1977. *Sov. Astr. Lett.*. 3:155 (orig. 1977. *Pis'ma Astron. Zh.* 3:291)
Vonlanthen P, Rauscher T, Winteler C, Puy D, Signore M, Dubrovich V. 2009. *Astron. Astrophys.* 503:47
Wharton L, Gold LP, Klemperer W. 1960. *J. Chem. Phys.* 33:1255
Watson WD. 1976. *Rev. Mod. Phys.* 48:513
Watson WD, Christensen RB, Deissler RJ. 1978. *Astron. Astrophys.* 65:159
Wolfe AM, Gawiser E, Prochaska JX. 2005. *Annu. Rev. Astron. Astrophys.* 43:861
Wong WY, Seager S, Scott D. 2006. *MNRAS* 367:1666
Wong WY, Moss A, Scott D. 2008. *MNRAS* 386:1023
Wrathmall SA, Gusdorf A, Flower DR. 2007. *MNRAS* 382:133
Yoneyama T. 1970. *Publ. Astron. Soc. Japan* 24:87
Yong D, Norris JE, Bessell MS, Christlieb N, Asplund M, et al. 2012. *arXiv1208.3016v1*
Yoon JS, Kim YW, Kwon DC, Song MY, Chang WS, et al. 2010. *Rep. Progr. Phys.* 73:116401
Yoshida N, Omukai K, Hernquist L, Abel T. 2006. *Ap. J.* 652:6
Yoshida N, Omukai K, Hernquist L. 2007. *Ap. J.* 667:L117
Zel'dovich YB, Kurt VG, Sunyaev RA. 1969. *Soviet Phys.-JETP Lett.* 28:146 (orig. 1968. *Zh. Eksp. Theor. Fiz.* 55:278)
Zel'dovich YB. 1978. *Sov. Astr. Lett.* 4:88 (orig. 1978. *Pis'ma Astron. Zh.* 4:165)
Zemke WT, Stwalley WC. 1980. *J. Chem. Phys.* 73:5584
Zinchenko I, Dubrovich V, Henkel C. 2011. *MNRAS* 415:L78
Zygelman B, Stancil PC, Dalgarno, A. 1998. *Ap. J.* 508:151